Astrocytic striatal GABA transporter activity governs dopamine release and shows maladaptive downregulation in early parkinsonism

Bradley M. Roberts[1], Natalie M. Doig[2], Katherine R. Brimblecombe[1,3], Emanuel F. Lopes[1], Ruth E. Siddorn[1], Sarah Threlfell[1,3], Natalie Connor-Robson[1,3], Nora Bengoa-Vergniory[1,3], Nicholas Pasternack[1], Richard Wade-Martins[1,3], Peter J. Magill[2,3] and Stephanie J. Cragg[1,3*]

Affiliations:

[1] Centre for Integrative Neuroscience, Department of Physiology, Anatomy and Genetics, University of Oxford, Oxford, United Kingdom

[2] Medical Research Council Brain Network Dynamics Unit, University of Oxford, Oxford, United Kingdom

[3] Oxford Parkinson's Disease Centre, University of Oxford, Oxford, United Kingdom

***Correspondence should be addressed to:**

Professor Stephanie Cragg
Department of Physiology, Anatomy & Genetics
University of Oxford, OX1 3PT, UK
Phone: +44 1865 282513
Email: Stephanie.cragg@dpag.ox.ac.uk

Summary

Striatal dopamine (DA) is critical for action and learning. Recent data show DA release is under tonic inhibition by striatal GABA. Ambient striatal GABA tone on striatal projection neurons can be governed by plasma membrane GABA uptake transporters (GATs) on astrocytes. However, whether striatal GATs and astrocytes determine DA output are unknown. We reveal that DA release in mouse dorsolateral striatum, but not nucleus accumbens core, is governed by GAT-3 and GAT-1. These GATs are partly localized to astrocytes, and are enriched in dorsolateral striatum compared to accumbens core. In a mouse model of parkinsonism, GATs become downregulated and tonic GABAergic inhibition of DA release augmented, despite attenuated GABA co-release from dopaminergic axons. These data define previously unappreciated and important roles for GATs and astrocytes in determining DA release in striatum, and reveal that they underlie maladaptive plasticity in early parkinsonism that impairs DA output in vulnerable striatal regions.

Keywords

astrocytes, co-release, electrophysiology, dopamine, GABA receptor, GABA transporter, GAT, neuron-glia interactions, optogenetics, Parkinson's disease, release probability, striatum, tonic inhibition, voltammetry

Highlights:

1. GABA transporters set the level of GABA inhibition of DA output in dorsal striatum
2. Astrocytes facilitate DA release by limiting tonic GABA inhibition
3. Tonic GABA inhibition of DA release is augmented in mouse model of parkinsonism
4. DA and GABA co-release are reduced in mouse model of parkinsonism

Introduction

Dopamine (DA) release in the dorsal and ventral striatum plays key roles in action selection and motivation, and is dysregulated in diverse disorders including Parkinson's disease (PD) and addictions. Striatal DA release is gated locally by axonal mechanisms and striatal neuromodulators that regulate or even drive DA release (Schmitz et al., 2003; Sulzer et al., 2016). It has recently been revealed that DA release is under tonic inhibition by striatal GABA (Lopes et al., 2018), operating through $GABA_A$ and $GABA_B$ receptors presumably located directly on DA axons (Lopes et al., 2018; Pitman et al., 2014; Schmitz et al., 2002). The striatum contains a high density of GABAergic projection neurons and interneurons and, in addition, receives a source of GABA co-released from mesostriatal DA neurons (Kim et al., 2015; Tritsch et al., 2012, 2014). Given the paucity of GABAergic synapses on DA axons (Charara et al., 1999), tonic inhibition of DA release by striatal GABA is presumably mediated through extrasynaptic effects of ambient GABA (Lopes et al., 2018). GABA can spill over for extrasynaptic actions in other nuclei (Farrant and Nusser, 2005), and in the dorsal striatum, provides a sizeable ambient GABA tone on spiny projection neurons (SPNs), evident as a tonic $GABA_A$ receptor-mediated inhibitory conductance (Ade et al., 2008; Cepeda et al., 2013; Kirmse et al., 2008, 2009; Santhakumar et al., 2010).

Tonic inhibition by ambient GABA across the mammalian brain is usually limited by uptake by plasma membrane GABA transporters (GATs) (Brickley and Mody, 2012). There are two isoforms of the GAT in striatum: GAT-1 (*Slc6a1*), abundant in axons of GABAergic neurons (Augood et al., 1995; Durkin et al., 1995; Ng et al., 2000; Yasumi et al., 1997); and GAT-3 (*Slc6a11*), expressed moderately (Ficková et al., 1999; Ng et al., 2000; Yasumi et al., 1997) and seen particularly on astrocytes (Chai et al., 2017; Ng et al., 2000; Yu et al., 2018). Emerging transcriptomic data indicate that striatal astrocytes might express both GAT-1 and GAT-3 (Chai et al., 2017; Gokce et al., 2016; Zhang et al., 2014). In addition, mRNA for GAT-1 and for GAT-3 has been found in midbrain DA neurons and these GATs have been suggested but not confirmed to be located on striatal DA axons to support GABA co-storage and co-release (Tritsch et al., 2014). Ambient GABA tone on SPNs in dorsal striatum is limited by the activity of GAT-3 and GAT-1 (Kirmse et al., 2008, 2009; Santhakumar et al., 2010; Wójtowicz et al., 2013), and recent evidence indicates that GAT-3 on striatal astrocytes play a particularly important role: GAT-3 dysregulation results in profound changes to SPN activity and striatum-dependent behavior (Yu et al., 2018). However, whether striatal GAT function is a critical for setting the level of DA output has not previously been examined.

Here we reveal that GAT-3 and GAT-1 strongly regulate striatal DA release in the dorsolateral striatum (DLS) but not in the nucleus accumbens core (NAcC), by limiting tonic inhibition by striatal ambient GABA. We identify a particular role for GATs located on striatal astrocytes in supporting DA release, and furthermore, reveal that maladaptive GAT regulation impairs DA output in the DLS in a mouse model of early parkinsonism.

RESULTS

DA release in DLS and NAcC is tonically inhibited by a GAD-dependent GABA source

We recently reported that axonal DA release in the dorsal striatum is under tonic inhibition by striatal GABA, as $GABA_A$ and $GABA_B$ receptor antagonists enhanced DA release evoked by single electrical and targeted light pulses (Lopes et al., 2018). Since mechanisms that regulate striatal DA release can diverge between dorsal and ventral striatal territories (Brimblecombe et al., 2015; Britt and McGehee, 2008; Janezic et al., 2013; Shin et al., 2017; Threlfell and Cragg, 2011; Threlfell et al., 2010), we determined whether DA release in NAcC, a part of the ventral striatum, is similarly regulated by tonic GABA inhibition. We used fast-scan cyclic voltammetry (FSCV) in acute coronal slices of mouse brain to detect extracellular concentration of DA ($[DA]_o$) at carbon-fiber microelectrodes evoked by single electrical pulses in DLS and NAcC (**Figure 1A**). Co-application of $GABA_A$ and $GABA_B$ receptor antagonists (+)-bicuculline (10 μM) and CGP 55845 (4 μM) respectively, significantly enhanced electrically evoked $[DA]_o$ by ~20% in either the DLS or NAcC, when compared to drug-free time-matched controls (DLS: $p = 0.0004$, n = 6 experiments/3 mice; NAcC: $p = 0.001$, n = 5 experiments/3 mice; **Figure 1B**). These effects were similar in DLS and NAcC (**Figure 1B**; $p > 0.9$; Mann-Whitney tests) and did not require striatal glutamate input (**Supplementary Figure S1**), nor cholinergic interneuron input to nAChRs (since experiments were conducted in the presence of the nAChR antagonist DHβE). Using an optogenetics-based strategy to activate DA axons selectively, we also confirmed that inhibition of DA release by GABA receptors does not require concurrent activation of striatal GABAergic microcircuits (**Figure 1C**). GABA receptor antagonism significantly enhanced $[DA]_o$ evoked by single light pulses by ~25% in both the DLS and NAcC compared to time-matched drug-free control (**Figure 1D**; DLS: $p < 0.0001$, n = 9 experiments/5 mice; NAcC: $p = 0.002$, n = 5 experiments/4 mice), and similarly so in DLS vs. NAcC (**Figure 1D**; $p > 0.9$; Mann-Whitney tests). These results confirm that DA release is under tonic inhibition by GABA in striatal regions spanning dorsal to ventral.

We tested whether GABAergic inhibition of DA release arose from GABA co-released by DA axons or from GABA originating from a canonical neuron source (i.e. striatal GABAergic neurons). Mesostriatal DA neurons synthesize, co-store and co-release GABA (Tritsch et al., 2012), with GABA synthesis depending on aldehyde dehydrogenase (ALDH)-1a1 (Kim et al., 2015). In contrast, canonical synthesis of GABA in neurons requires glutamic acid decarboxylase (GAD). We inhibited GABA synthesis in DA axons by pre-treating slices with ALDH inhibitor disulfiram (10 μM) for 2 to 4 hours, which depleted light-evoked GABA currents from DA axons onto SPNs by half (**Supplementary Figure S2**), as reported previously (Kim et al., 2015). However, ALDH inhibition did not prevent GABA receptor antagonists from enhancing DA release: in the DLS, in the presence of disulfiram, GABA receptor antagonists enhanced light-evoked $[DA]_o$ by ~40%, which was a significantly larger effect than seen without disulfiram (**Figure 1E**; with disulfiram versus without, $p = 0.005$, Mann-Whitney test; disulfiram present: n = 6 experiments/5 mice; disulfiram absent: n = 10 experiments/7 mice). These data suggest that GABA co-released from DA axons does not directly inhibit DA release. They also suggest that ALDH-dependent GABA acts indirectly to limit tonic inhibition by a different, ALDH-

independent source. To assess whether tonic inhibition of DA release depended instead on a GAD-dependent GABA source, we pre-treated brain slices with GAD inhibitor 3-mercaptopropionic acid (3-MPA, 500 μM) for 2 to 4 hours, which attenuates electrically evoked GABA transmission onto SPNs by more than half (Kim et al., 2015). After GAD inhibition, the disinhibition of DA release in the DLS by GABA receptor antagonists was attenuated (**Figure 1E**; with 3-MPA vs. without, $p = 0.008$, Mann-Whitney test; 3-MPA: n = 7 experiments/5 mice; 3-MPA absent: n = 10 experiments/7 mice), indicating that a GAD-dependent GABA source provides tonic inhibition of striatal DA release.

GAT-1 and GAT-3 inhibition attenuates DA release in the DLS but not NAcC

Given the paucity of GABAergic axoaxonic synapses identified on DA axons (Charara et al., 1999), tonic inhibition of DA release likely arises from extrasynaptic ambient GABA. We tested the hypothesis that GAT, through its ability to govern ambient GABA (Kirmse et al., 2008, 2009; Santhakumar et al., 2010; Wójtowicz et al., 2013), determines the level of tonic inhibition of DA release. The non-selective GAT inhibitor (±)-nipecotic acid (NPA) (1 - 10 mM) inhibits all subtypes of GATs (Goubard et al., 2011; Li et al., 2017). Bath application of NPA (1.5 mM) attenuated evoked $[DA]_o$ in the DLS to ~60% of time-matched controls (**Figure 2A**; electrical: $p < 0.0001$, Mann-Whitney test, n = 9 experiments/5 mice; **Figure 2B**; light: $p = 0.006$, Mann-Whitney test, n = 9 experiments/5 mice). NPA attenuated evoked $[DA]_o$ to a greater extent in DLS than in NAcC (**Figure 2D**; DLS vs NAcC, $p = 0.0008$, Mann-Whitney test) where the effect of NPA on electrically evoked $[DA]_o$ did not reach statistical significance compared to time-matched controls (**Figure 2C**; $p = 0.06$, Mann-Whitney test; n = 6 experiments/4 mice). These data indicate that the level of tonic inhibition of DA release is limited by GAT in DLS, and to a greater degree than in NAcC.

Two main isoforms of the GAT are expressed in the basal ganglia: GAT-1 and GAT-3 (Jin et al., 2011). We identified which isoform(s) limits GABAergic inhibition of DA release in the DLS, using selective inhibitors. The GAT-1 selective inhibitor SKF89976A (20 μM) significantly attenuated electrically evoked $[DA]_o$ in DLS to ~75% of time-matched controls (**Figure 2E;** $p = 0.0004$, Mann-Whitney test, n = 6 experiments/4 mice). Combined inhibition of GAT-1 and GAT-3 with SKF89976A plus SNAP5114 (50 μM) significantly attenuated electrically evoked $[DA]_o$ to ~60% of time-matched controls (**Figure 2F;** $p < 0.0001$, Mann-Whitney test, n = 9 experiments/5 mice), an additional effect compared to GAT-1 inhibition alone and equivalent to that seen with broad-spectrum GAT inhibitor NPA (**Figure 2G**; Kruskal-Wallis ANOVA, $p = 0.003$; SKF+SNAP vs. SKF: $p < 0.05$, NPA vs. SKF+SNAP: $p > 0.05$, NPA vs. SKF: $p < 0.05$, Dunn's multiple comparison tests). These data indicate that both GAT-1 and GAT-3 limit the level of GABA inhibition of DA release in the DLS.

GAT inhibition attenuates striatal DA release by increasing GABA receptor tone

We ruled out diminished DA storage as a cause of the attenuation of DA release following GAT inhibition: Striatal DA content measured using high performance liquid chromatography (HPLC) with electrochemical detection was unchanged after incubation in NPA compared to controls (**Figure 2H;** $p = 0.60$, Mann-

Whitney test, n = 19 experiments/5 mice per condition). Instead, we confirmed that GAT inhibition modified DA release in a GABA receptor-dependent manner. The acute effects of NPA on evoked $[DA]_o$ were prevented in the presence of antagonists for $GABA_A$ and $GABA_B$ receptors combined (picrotoxin, 100 μM, CGP55845, 4 μM) (**Figure 2I;** without GABA receptor antagonists: ~65% of baseline; with GABA receptor antagonists: ~95% of baseline; p = 0.001, Mann-Whitney test, n = 5 experiments/4 mice), consistent with the effects of GAT on DA release being mediated via extracellular GABA acting on GABA receptors. We have previously shown that activation of GABA receptors can slightly modify the activity-dependence of DA release during short stimulus trains (Lopes et al., 2018). Consistent with an increase in GABA receptor activation, GAT inhibitor NPA increased the dependence of evoked $[DA]_o$ on pulse number during 50 Hz trains in DLS (**Figure 2J;** F = 434.7, p < 0.0001, drug condition x pulse no. interaction, two-way repeated-measures ANOVA; 2p: p = 0.004, 5p: p < 0.0001, 10p: p < 0.0001; Sidak's multiple comparisons; n = 8 experiments/5 mice). NPA also increased the paired-pulse ratio of electrically evoked $[DA]_o$ at short inter-pulse intervals (**Supplementary Figure S3**) consistent with a decrease in DA release probability (Jennings et al., 2015). Together these data indicate that GAT inhibition attenuates DA release through increasing GABA receptor tone.

We assessed whether the greater effect of GAT inhibition in DLS than NAcC (see Figure 2) was due to differences in GABA receptor function between regions. However, bath application of exogenous GABA (2 mM) attenuated $[DA]_o$ evoked by 1p electrical stimulation to a similar degree in DLS and NAcC (**Figure 2K;** DLS vs. NAcC: p = 0.33, Mann-Whitney test, DLS n = 6 experiments/4 mice, NAcC, n = 5 experiments/4 mice), ruling out overall differences in GABA receptor function as a factor. These findings suggest that the function of GAT in limiting tonic inhibition differs between DLS and NAcC.

GAT-3 and GAT-1 function and expression is enriched in DLS versus NAcC

To identify whether GAT regulates tonic GABA inhibition to a greater degree in DLS than NAcC, we recorded the tonic $GABA_A$ receptor-mediated currents in SPNs using whole-cell voltage-clamp electrophysiology and assessed the impact of GAT inhibition on holding current. We confirmed that changes in holding current were mediated by $GABA_A$ receptors by subsequently applying $GABA_A$ antagonist picrotoxin (PTX; 100 μM). Consistent with the effects on DA release, GAT inhibition with NPA (1.5 mM) elicited a significantly greater increase in $GABA_A$-mediated holding current in SPNs in the DLS than in the NAcC (**Figure 3A-C;** DLS vs NAc: p = 0.008, Mann-Whitney test; DLS: p = 0.0003, Friedman's ANOVA on Ranks, NPA vs. drug-free baseline: p = 0.001, NPA + PTX vs. drug-free baseline: p = 0.16, NPA vs. NPA + PTX: p < 0.001, Student-Newman-Keuls tests, n = 7 cells/5 mice; NAcC: p = 0.0001, Friedman's ANOVA on Ranks, NPA vs. drug-free baseline: p = 0.014, NPA + PTX vs. drug-free baseline: p = 0.014, NPA vs. NPA + PTX: p = 0.002, Student-Newman-Keuls tests, n = 6 cells/3 mice). These data corroborate a greater role for GATs in limiting ambient GABA tone in DLS than in NAcC.

Furthermore, tonic GABA inhibition of SPNs in DLS, like DA release, was regulated by both GAT1 and GAT3. Inhibition of GAT-1 alone with SKF89976A (20 μM) induced a small increase in the $GABA_A$-mediated holding current (**Figure 3D,** p = 0.006, Friedman's ANOVA on Ranks, SKF vs. drug-free baseline: p = 0.001, SKF + PTX vs. drug-free baseline: p = 0.41, SKF vs. SKF + PTX: p = 0.01, Student-Newman-Keuls tests, n = 6 cells/3 mice). Combined inhibition of GAT-1 and GAT-3 with SKF89976A (20 μM) and SNAP5114 (50 μM) induced a three-fold increase (**Figure 3E;** p = 0.006, Friedman's ANOVA on Ranks, SKF + SNAP vs. drug-free baseline: p = 0.001, SKF + SNAP + PTX vs. drug-free baseline: p = 0.41, SKF + SNAP vs. SKF + SNAP + PTX: p = 0.011, Student-Newman-Keuls tests, n = 6 cells/4 mice), which was greater than after GAT-1 inhibition alone, but similar to that seen with broad-spectrum GAT inhibition (**Figure 3F;** p = 0.0002, Kruskal-Wallis analysis of variance; SKF + SNAP vs. SKF: $p < 0.01$, NPA vs. SKF + SNAP: $p > 0.05$, NPA vs. SKF: $p < 0.01$; Dunn's multiple comparison tests).

GABA tone in striatum has previously been reported to be action-potential independent i.e. due to spontaneous GABA release (Wójtowicz et al., 2013). We assessed whether GATs were limiting an action potential-independent GABA tone. In the presence of Na_v blocker tetrodotoxin (TTX, 1 μM), NPA increased the $GABA_A$-mediated holding current in SPNs in the DLS (**Figure 3G,** NPA vs. baseline: p = 0.03, Wilcoxon signed-rank test; n = 6 cells/3 mice) to a level not different to that induced by NPA in TTX-free conditions (**Figure 3H;** p = 0.43, Mann-Whitney test), confirming that GATs in DLS are limiting a spontaneous GABA tone.

Collectively, these results show that striatal GAT-1 and GAT-3 regulate an ambient GABA tone, which arises from an action-potential independent source, and do so to a greater degree in DLS compared to NAcC. We explored an anatomical basis for the regional heterogeneity in GAT function. Striatal immunoreactivity to GAT-1 and GAT-3 in the DLS and NAcC revealed relative enrichment in the DLS for both GAT1 (**Figure 4A,B,** p = 0.009, Wilcoxon signed-rank test, n = 12 hemispheres/6 mice) and GAT-3 (**Figure 4C,D**; p = 0.002, Wilcoxon signed-rank test, n = 12 hemispheres/6 mice). We also noted enriched GAT-3 in the medial NAc shell (NAcS) contiguous with the medial septal nucleus (**Supplementary Figure S4**). This observation prompted us to identify the effects of GAT inhibition on DA release in NAcS. Correspondingly, we noted that GAT inhibition diminished electrically evoked $[DA]_o$ in NAcS, unlike NAcC (**Supplementary Figure S4**), indicating further regional heterogeneity in the role of GATs in limiting tonic inhibition across the striatum.

GAT-1 and GAT-3 on astrocytes are key regulators of ambient GABA inhibition of DA release

Striatal GATs are located on the plasma membranes of a variety of cells that include GABAergic neurons (Augood et al., 1995; Durkin et al., 1995; Ng et al., 2000; Yasumi et al., 1997) and astrocytes (Chai et al., 2017; Ng et al., 2000; Yu et al., 2018). GATs have also been presumed, but not confirmed, to reside on DA axonal membranes to support GABA uptake, co-storage and co-release (Tritsch et al., 2014). To better understand where GAT is located to regulate tonic GABAergic inhibition of DA, we probed two candidate

locations, namely DA axons, and astrocytes. We explored whether GAT-1 or GAT-3 could be detected on DA axons using immunofluorescence and confocal microscopy, but we did not find robust evidence for localization of these proteins to DA axons identified by an eYFP reporter (**Supplementary Figure S5**). As a positive control for our immunofluorescence and imaging, we confirmed that GAT-1 was localized to the neurites of parvalbumin-expressing GABAergic interneurons (**Supplementary Figure S6**), which are well known to express GAT-1 (Augood et al., 1995). Our observations do not provide support for the assumption that GAT-1 and GAT-3 proteins are localized to DA axons (Tritsch et al., 2014) in order to provide GABA uptake for co-storage and co-release.

In many brain regions, including striatum, astrocytes are thought to regulate ambient GABA levels by active uptake of GABA (Yu et al., 2018). GAT-3 protein expression has been documented on striatal astrocytes (Chai et al., 2017; Ng et al., 2000; Yu et al., 2018), and although GAT-1 is typically associated with neuronal structures (Borden, 1996), recent transcriptomic studies have found RNA for both GAT-3 and GAT-1 in striatal astrocytes (Chai et al., 2017; Gokce et al., 2016; Zhang et al., 2014). We revisited GAT-1 localization, using immunofluorescence and confocal microscopy with antibodies directed against GAT-1 or GAT-3, as well as against the striatal astrocytic marker S100β (Chai et al., 2017) in the DLS and NAcC (**Figure 5A**,**B**). As expected, we found that GAT-3 was robustly co-localized to the plasma membranes of S100β-expressing astrocytes (**Figure 5C**, n = 3 mice). We also found some instances of localization of GAT-1 on S100β astrocytes (**Figure 5D**, n = 3 mice). These data indicate that, although GAT-1 is commonly expressed by striatal GABAergic interneurons, GAT-1 can also be expressed by some astrocytes in striatum.

We next probed whether GATs on striatal astrocytes could govern tonic GABAergic inhibition of DA release. To address this, we pre-treated striatal slices with fluorocitrate (200 µM for >1hr, or vehicle control), an established approach for metabolically inhibiting astrocytes, thus rendering them inactive and preventing the effects of astrocytic GAT (Boddum et al., 2016; Bonansco et al., 2011). DA release in fluorocitrate- and vehicle-treated slices was then recorded with/without the GAT inhibitor NPA. We first confirmed that we could detect the effects of GAT inhibition on DA release in DLS in control slices. Accordingly, $[DA]_o$ evoked by 1p electrical stimulation across a range of sites in the DLS from slices incubated in NPA (1.5 mM) for 30 min was significantly less than in NPA-free control conditions, as expected (**Figure 5E;** p = 0.0003, Mann-Whitney test; n = 24 observations/5 mice for each condition), and 4p/1p ratio (50 Hz) was appropriately enhanced (**Figure 5F;** p = 0.014, Mann-Whitney test; n = 8 experiments/5 mice for each condition). By contrast, in slices pre-treated with fluorocitrate to inactivate astrocytes, NPA did not significantly modify $[DA]_o$ evoked by 1p (**Figure 5G;** p = 0.10, Mann-Whitney test, n = 42 observations/7 mice for each condition), or the 4p/1p ratio (50 Hz), compared to NPA-free conditions (**Figure 5H;** p = 0.64, Mann-Whitney test, n = 13 observations/7 mice for each condition). We noted also that evoked $[DA]_o$ was lower in fluorocitrate-treated vs vehicle-treated slices (**Figure 5I;** p = 0.0001, Mann-Whitney test). Additionally, the inhibition of $[DA]_o$ by NPA was attenuated when astrocytes were inhibited

compared to not (**Figure 5J;** p = 0.004, Mann-Whitney test). Together, these data indicate that GATs on striatal astrocytes regulate the level of inhibition of DA release by ambient GABA.

Tonic inhibition of DA release in the DLS is augmented in a mouse model of parkinsonism

Our data described above provide compelling evidence that GATs regulate DA output in the DLS. Intriguingly, dysregulation of GATs within the basal ganglia has been implicated in models of neurological disease: in a 6-hydroxydopamine-induced mouse model of Parkinson's, astrocytes in the external globus pallidus have downregulated GAT-3 (Chazalon et al., 2018); and in R6/2 and FVB/N transgenic mouse models of Huntington's disease, GAT expression in striatum is increased and tonic inhibition by ambient GABA decreased (Cepeda et al., 2013; Wójtowicz et al., 2013; Yu et al., 2018). Given that deficits in DA transmission occur in dorsal striatum, but not in NAcC, in several transgenic rodent models of early parkinsonism prior to cell loss (Janezic et al., 2013; Sloan et al., 2016; Taylor et al., 2014), we explored whether tonic GABAergic inhibition of striatal DA release and its regulation by striatal GAT might be affected in a mouse model of early parkinsonism.

We chose to use *SNCA*-OVX mice, a model of early parkinsonism (Janezic et al., 2013). *SNCA*-OVX mice are devoid of mouse α-synuclein but overexpress human wildtype α-synuclein at disease-relevant levels and show early deficits in DA release prior to DA cell loss (Janezic et al., 2013). To address our aims, we made these *SNCA*-OVX mice 'optogenetics capable', such that they allowed for optical manipulation of DA axons. We crossed *Slc6a3*$^{IRES\text{-}Cre}$ mice with α-synuclein knockout mice to create *Slc6a3*$^{IRES\text{-}Cre}$ mice devoid of mouse α-synuclein, and then crossed these mice with S*NCA*-OVX mice to generate two cohorts of mice, both devoid of mouse α-synuclein: (1) "*SNCA*+" mice that express Cre recombinase in DA neurons and human α-synuclein; and (2) as littermate background controls, "Snca-/-" mice that express Cre recombinase in DA neurons but no human transgene. We confirmed that, as observed in the original *SNCA*-OVX mice (Janezic et al., 2013), the resulting *SNCA*+ mice at 4 months exhibited a ~30% deficit in electrically evoked $[DA]_o$ when compared to littermate controls (*Snca*-/-) in the dorsal striatum (**Figure 6A;** t = 3.3, df = 46, p = 0.002, unpaired t test; n = 24 observations/5 mice for each genotype) and not in the NAc (**Figure 6A;** t = 1.4, df = 40, p = 0.17, unpaired t-test; n = 21 observations/5 mice for each genotype). The DA release deficit in dorsal striatum was not attributable to a reduction in striatal DA content in *SNCA*+ mice compared to *Snca*-/- mice (**Figure 6B;** t = 0.16, df = 14, p = 0.87, dorsal striatum; t = 0.74, df = 14, p = 0.47, NAc; n = 8 experiments/5 mice for each genotype). We then established that $[DA]_o$ evoked optogenetically in DLS by single light pulses also showed a similar deficit in *SNCA*+ compared to Snca-/- (**Figure 6C**; t = 2.44, df = 29, p =0.02; *SNCA+*: n = 16 observations/3 mice; Snca-/-: n = 15 observations/3 mice).

Furthermore, this new optogenetic capable model of parkinsonism allowed us to address for the first time whether DA release deficits in DLS are accompanied by corresponding deficits in GABA co-release from DA axons. To provide a readout of GABA co-release, we used voltage-clamp recordings of currents evoked in SPNs by optical stimulation of DA axons (**Figure 6D**). We observed a significantly lower amplitude

of light-evoked GABAergic co-release currents in SPNs of *SNCA+* mice compared to *Snca-/-* mice (**Figure 6D,E**; t = 2.68, df = 14, p = 0.018; *SNCA+*: n = 9 cells/4 mice, *Snca-/-*: n = 7 cells/4 mice). These evoked currents were $GABA_A$ receptor-mediated as they were eliminated by picrotoxin (PTX, 100 μM) (**Figure 6F**; t = 4.55, df = 10, p = 0.001). This observed difference in GABAergic current amplitudes was not due to differences in series resistance (**Figure 6G;** t = 0.23, df = 14, p = 0.82).

We then explored whether tonic GABA inhibition of DA release was modified in the parkinsonian model in DLS and NAcC. We found that $GABA_R$ antagonism enhanced $[DA]_o$ evoked by single light pulses to a significantly greater degree in *SNCA+* mice than in *Snca-/-* controls in DLS (**Figure 6H;** p = 0.0003, Mann-Whitney test; *SNCA+*: n = 8 experiments/5 mice, *Snca-/-*: n = 7 experiments/5 mice) but not in NAcC (**Figure 6I**; p = 0.09, Mann-Whitney test; *SNCA+*: n = 8 experiments/5 mice, *Snca-/-*: n = 9 experiments/5 mice), which was a significant regional difference (**Figure 6J**; p = 0.02, Mann-Whitney test). These data indicate that the GABA tone on DA axons is dysregulated in *SNCA+* parkinsonian mice and in particular, that tonic GABAergic inhibition of DA release is augmented in DLS.

We tested the hypothesis that elevated tonic inhibition of DA release in the DLS of *SNCA+* mice might be due to impaired GAT function. We tested the effect of the non-selective GAT inhibitor NPA on $[DA]_o$ evoked by single electrical pulses in DLS and found an attenuated effect of NPA in *SNCA+* versus *Snca-/-* controls (**Figure 6K;** p = 0.03, Mann-Whitney test vs *Snca -/-*; n = 5 experiments/4 mice for each genotype). Quantification of Western blots of dorsal striatal tissue revealed lower levels of both GAT-1 and GAT-3 proteins in *SNCA+* mice versus *Snca-/-* controls (**Figure 6L;** GAT-1: p = 0.0004; GAT-3: p = 0.01; Mann-Whitney tests; n = 7 *SNCA+* mice, n = 10 *Snca -/-* mice). Taken together, these data suggest that tonic inhibition of DA release by ambient GABA is augmented in the dorsal striatum in early parkinsonism due to decreased GAT-1 and GAT-3 (**Figure 7**).

DISCUSSION

We define a major role for striatal GATs and astrocytes in setting the level of DA output in the striatum. We show that GAT-1 and GAT-3, located at least in part on striatal astrocytes, govern tonic GABAergic inhibition of DA release. GATs operate in a heterogeneous manner across the striatum, substantially limiting tonic inhibition of DA release in DLS but not NAcC. Moreover, in a mouse model of early parkinsonism prior to the overt loss of DA neurons, we reveal maladaptive decreases in striatal GAT-1 and GAT-3 expression and consequently, profound augmentation of tonic inhibition of DA release by GABA in the dorsal striatum.

GATs limits the tonic inhibition of DA release

We found that tonic inhibition of DA release by GABA spans dorsal-ventral territories of striatum and arises from a GAD-dependent source of GABA. The source of GABA was not ALDH-dependent e.g. co-release from DA axons, as inhibition of ALDH did not attenuate the tonic inhibition of DA release by GABA, despite attenuating GABA co-release from DA axons, as seen previously (Kim et al., 2015). Conversely, ALDH-

inhibition slightly boosted tonic inhibition of DA release, suggesting that ALDH-dependent sources of GABA, such as GABA co-release from DA axons, limit the tonic inhibition by the GAD-dependent GABA network. Correspondingly, in mice expressing human α-synuclein, in which we found that GABA co-release from DA axons is attenuated, we also found that the level of tonic GABA inhibition on DA release was boosted. We note that *Aldh1a1* mutations in humans and deletion in mice lead to alcohol-consuming preferences (Kim et al., 2015; Liu et al., 2011; Sherva et al., 2009), and speculate that a modified DA output might plausibly contribute to this behaviour.

The paucity of GABAergic synapses on DA axons (Charara et al., 1999) suggests that GAD-dependent GABA tone arises from the extrasynaptic ambient tone that can be detected in striatum (Ade et al., 2008; Cepeda et al., 2013; Kirmse et al., 2008, 2009; Santhakumar et al., 2010). This tone was action potential-independent, i.e. spontaneous (Kaeser and Regehr, 2013), as reported previously for tonic inhibition of SPNs (Wójtowicz et al., 2013). A spontaneous GABAergic regulation of DA release is not surprising when considering that the axonal arbour of a given nigrostriatal DA neuron (in rat) reaches on average 2.7% of the volume of striatum (Matsuda et al., 2009; Oorschot, 1996), and that such volumes contain ~74,000 GABAergic neurons (calculated from 2.8 million striatal neurons per hemisphere (Oorschot, 1996) of which ~98% are GAD-immunoreactive) and also GAD-positive cholinergic interneurons that can co-release GABA (Lozovaya et al., 2018). Even very low rates of spontaneous vesicle release from a small fraction of GAD-utilizing GABAergic neurons might summate sufficiently to provide a tone at GABA receptors on DA axons that limits DA output. The general functions of this spontaneous GABA tone are not well understood, but could differ from functions of action potential-dependent or synaptic events (Farrant and Nusser, 2005), and could include regulation of DA axonal membrane resistance to modify the impact of other inputs or limit the propagation of action potentials through the axonal arbour for a sparser coding.

We found that GAT-1 and GAT-3 both limit the actions of GABA on DA axons in DLS, and thereby indirectly facilitate DA release. This unprecedented role for the GATs in supporting DA output was heterogeneous: GATs limited tonic GABAergic inhibition of DA release in DLS, and also NAcS, but not NAcC, which corresponded with heterogeneity in GAT-1 and GAT-3 expression. Of note, the positive relationship we find between GAT function and DA output is paralleled by, and provides a candidate explanation for, some clinical effects of GAT inhibitors e.g. tiagibine. When used clinically as antiepileptics drugs to increase extracellular GABA levels, these inhibitors can have parkinsonian-like motor side effects (Zaccara et al., 2004).

We did not find evidence for robust localization of GAT-1 or GAT-3 to DA axons in DLS, despite a previous inference that GATs reside on DA axons to support GABA uptake for co-release (Tritsch et al., 2014). This inference was based on mRNA for GAT-1 (and weakly for GAT-3) being present in the somata of DA neurons in substantia nigra, and on the attenuation of GABA co-release from DA axons after pharmacological inhibition of GATs (Tritsch et al., 2014). However, because subsequent work has shown that there is a tonic GABAergic inhibition of DA release mediated by both $GABA_A$ and $GABA_B$ receptors

(Lopes et al., 2018), which we show here is profoundly limited by the GATs, then the observed dependence of GABA co-release on GAT is very likely a result of the GATs limiting tonic inhibition of GABA co-release, rather than GATs necessarily being required for GABA uptake.

We revealed that astrocytes play a critical role in limiting the tonic inhibition of DA release and therefore supporting DA output. We found that both GAT-3 and, to a lesser extent, GAT-1, could be identified on astrocytes, challenging the previous generalization that GAT-1 is exclusively neuronal (Borden, 1996). The role we find for astrocytes in supporting GABA uptake to minimise tonic inhibition of DA release, indicates a previously unappreciated role for astrocytes in determining the dynamic output of DA. This finding significantly revises current understanding of the striatal mechanisms that can dynamically regulate DA transmission. Astrocytic GATs have recently been shown to regulate tonic GABAergic inhibition of striatal SPNs and striatal-dependent behaviours (Yu et al., 2018), and thus, our collective findings point to GATs and astrocytes as powerful regulators of striatal and DA function that warrant further future investigation.

Striatal GAT dysfunction in a mouse model of Parkinson's disease

To probe the significance of the regulation of striatal DA by striatal GATs, we explored GAT function in a mouse model of early parkinsonism. A recent study in external globus pallidus of dopamine-depleted rats found elevated extracellular GABA resulting from downregulation of GAT-3 on astrocytes, mediated through a loss of DA signalling at D_2 DA receptors (Chazalon et al., 2018). Conversely, striatal GAT-3 levels are upregulated in mouse models of Huntington's disease (Wójtowicz et al., 2013; Yu et al., 2018). We explored potential adaptations to GAT function and tonic GABA inhibition of DA release in the striatum of the human α-synuclein-overexpressing mouse model of PD. This model is a highly physiological, slowly progressing mouse model of parkinsonism, that, in capturing a human disease-relevant genetic burden of α-synuclein overexpression, shows early deficits in DA release restricted to dorsal striatum prior to late-stage degeneration of DA neurons, disturbed encoding of behaviour of surviving DA neurons and a motor phenotype (Dodson et al., 2016; Janezic et al., 2013). We firstly ascertained the novel finding that DA transmission deficits in this model in early adulthood are accompanied by a corresponding deficit in GABA co-release from DA axons, which suggests that in early parkinsonism at least, malfunction in nigrostriatal DA is accompanied by malfunction in nigrostriatal GABA. Furthermore, we found an augmentation of tonic GABA inhibition of DA release in the DLS (and not NAcC), which was accompanied by downregulated GAT-1 and GAT-3 expression. Whether these adaptations in GAT are consequential to reduced dopamine signalling, as seen in the globus pallidus after massive depletion of dopamine (Chazalon et al., 2018), or due to a potential interaction between α-synuclein and striatal GAT and/or astrocytes is not yet known. Regardless, this resulting enhanced tonic inhibition will diminish nigrostriatal DA release, compounding any release deficits underpinned by α-synuclein actions e.g. tighter vesicle clustering at DA release sites (Janezic

et al., 2013). These changes in GATs and tonic GABA inhibition in early parkinsonism can be considered 'maladaptive'.

In conclusion, the regulation of striatal GABA-DA interactions via striatal GATs and astrocytes represent loci for governing DA output as well as for maladaptive plasticity in early parkinsonism, which could also provide a novel therapeutic avenue for upregulating DA signalling in PD.

MATERIALS AND METHODS

Mice. All experimental procedures involving the use of animals were carried out according to institutional guidelines and conformed to the UK Animals (Scientific Procedures) Act 1986. Wild-type C57BL/6J mice were obtained from Charles River (Harlow, UK). Knock-in mice bearing an internal ribosome entry site (IRES)-linked Cre recombinase gene downstream of the gene *Slc6a3*, which encodes the plasma membrane dopamine transporter (DAT) were obtained from Jackson Laboratories (*Slc6a3*$^{IRES\text{-}Cre}$ mice; *B6.SJL-Slc6a3*$^{tm1.1(cre)Bkmn}$/J; stock no. 006660). PV^{Cre} knock-in mice expressing Cre recombinase in parvalbumin (PV)-expressing neurons were obtained from Jackson Laboratories (*B6;129P2-Pvalb*$^{tm1(cre)Arbr}$/J; stock no. 008069). BAC-transgenic mice that overexpress human α-synuclein (*SNCA*) at Parkinson's disease-relevant levels and are back-crossed onto an α-synuclein-null (*Snca*$^{-/-}$) background (B6.Cg-Tg(*SNCA*)OVX37Rwm Snca^{tm1Rosl}/J; Jackson Laboratories stock no. 023837), "*SNCA*-OVX" mice, were bred locally (Janezic et al., 2013). 'Optogenetic capable' *SNCA+* mice were generated by crossing *Slc6a3*$^{IRES\text{-}Cre}$+/+; *Snca*-/- mice with *SNCA*+/-; *Snca*-/- mice (*SNCA*-OVX mice) (Janezic et al., 2013). For all experiments involving *SNCA*+ mice, we used age- and sex-matched *Snca*-null mice (heterozygous for Slc6a3$^{IRES\text{-}Cre}$) as littermate controls. All mice were maintained on a C57BL/6 background, group-housed and maintained on a 12-hr light cycle with *ad libitum* access to food and water. All transgenic mice used in experiments were homozygous for transgenes or mutant alleles.

Stereotaxic intracranial injections. Slc6a3$^{IRES\text{-}Cre}$ mice, PV^{cre} mice (postnatal day (P) 28 – 35) and Slc6a3$^{IRES\text{-}Cre}$ x *SNCA*-OVX mice (P 77 - 84) were anesthetized with isoflurane and placed in a small animal stereotaxic frame (David Kopf Instruments). After exposing the skull under aseptic techniques, a small burr hole was drilled and adeno-associated virus (8x10^{12} genome copies per ml; UNC Vector Core Facility) encoding Cre-dependent ChR2 was injected. Viral solutions were injected at an infusion rate of 100 nL/min with a 32-gauge Hamilton syringe (Hamilton Company) and withdrawn 5-10 min after the end of injection. In Slc6a3$^{IRES\text{-}Cre}$ x *SNCA*-OVX mice, and Slc6a3$^{IRES\text{-}Cre}$ mice, a total volume of 1 µL of AAV5-EF1α-DIO-hChR2(H134R)-eYFP was injected bilaterally (500 nL per hemisphere/injection) into substantia nigra pars compacta (SNc, AP -3.1 mm, ML ±1.2 mm from bregma, DV -4.25 mm from exposed dura mater). In PV-Cre mice, a total volume of 600 nL of AAV2-EF1α-DIO-hChR2(H134R)-eYFP was injected bilaterally (300 nL per hemisphere/injection) into dorsolateral striatum (DLS, AP +0.65 mm, ML ±2.0 mm from bregma, DV -1.85

mm from exposed dura mater). Viral-injected mice were used for experiments after >28 days post-injection.

Slice preparation. Acute brain slices were obtained from 35- to 80-day-old mice using standard techniques. Mice were culled by cervical dislocation (for FSCV experiments alone) or mice were anaesthetized with pentobarbital and transcardinally perfused with ice-cold artificial cerebrospinal fluid (aCSF) containing (in mM): 130 NaCl, 2.5 KCl, 26 $NaHCO_3$, 2.5 $CaCl_2$, 2 $MgCl_2$, 1.25 NaH_2PO_4 and 10 glucose (for whole-cell patch-clamp electrophysiology experiments alone or in combination with FSCV experiments). 300 µm-thick coronal slices containing caudate putamen (CPu) and NAc were prepared from dissected brain tissue using a vibratome (VT1200S, Leica Microsystems) and transferred to a holding chamber containing a HEPES-based buffer solution maintained at room temperature (20-22°C) containing (in mM): 120 NaCl, 20 $NaHCO_3$, 10 glucose, 6.7 HEPES acid, 5 KCl, 3.3 HEPES sodium salt, 2 $CaCl_2$, 2 $MgSO_4$, 1.2 KH_2PO_4 (for FSCV experiments alone) or containing aCSF kept at 34°C for 15 min before returning to room temperature (20-22°C). All recordings were obtained within 5-6 hours of slicing. All solutions were saturated with 95% O_2 / 5% CO_2.

Fast-scan cyclic voltammetry (FSCV). Individual slices were hemisected and transferred to a recording chamber and superfused at ~3.0 mL/min with aCSF at 31-33 °C. A carbon fibre microelectrode (CFM; diameter 7- 10 µm, tip length 70-120 µm), fabricated in-house, was inserted 100 µm into the tissue and slices were left to equilibrate and the CFM to charge for 30-60 min prior to recordings. All experiments were carried out either in the dorsolateral quarter (DLS) of the CPu or nucleus accumbens (NAc) core (NAcC; within 100 µm of the anterior commissure) or lateral NAc shell (NAcS), one site per slice (see Supplementary Figure S4). Evoked extracellular DA concentration ($[DA]_o$) was measured using FSCV at CFMs as described previously (Threlfell et al., 2012). In brief, a triangular voltage waveform was scanned across the microelectrode (-700 to +1300 mV and back vs Ag/AgCl reference, scan rate 800 V/s) using a Millar Voltammeter (Julian Millar, Barts and the London School of Medicine and Dentistry), with a sweep frequency of 8 Hz. Electrical or light stimuli were delivered to the striatal slices at 2.5 min intervals, which allow stable release to be sustained at ~90-95% (see Fig. 1B,D) over the time course of control experiments. Evoked currents were confirmed as DA by comparison of the voltammogram with that produced during calibration with applied DA in aCSF (oxidation peak +500-600 mV and reduction peak -200 mV). Currents at the oxidation peak potential were measured from the baseline of each voltammogram and plotted against time to provide profiles of $[DA]_o$ versus time. CFMs were calibrated *post hoc* in 2 µM DA in each experimental solution. Calibration solutions were made immediately before use from stock solution of 2.5 mM DA in 0.1 M $HClO_4$ stored at 4 °C. CFM sensitivity to DA was between 10 and 40 nA/µM. Unless noted otherwise, FSCV recordings were carried out in the presence of dihydro-β-erythroidine (DHβE, 1 µM), an antagonist at β2 subunit-containing nicotinic acetylcholine receptors (nAChRs), to eliminate cholinergic

signalling effects on DA release (Exley and Cragg, 2008; Rice and Cragg, 2004; Threlfell et al., 2012). Release was tetrodotoxin-sensitive as shown previously (Threlfell et al., 2012).

In experiments where $[DA]_o$ was evoked by electrical stimulation, a local bipolar concentric Pt/Ir electrode (25 µm diameter; FHC Inc.) was placed approximately 100 µm from the CFMs and stimulus pulses (200 µs duration) were given at 0.6 mA (perimaximal in drug-free control conditions). We applied either single pulses (1p) or 2-10 pulses (2p, 4p, 5p, 10p) at 10 - 100 Hz. A frequency of 100 Hz is useful as a tool for exposing changes in short-term plasticity in DA release that arise through changes in initial release probability (Jennings et al., 2015; Rice and Cragg, 2004). In experiments where $[DA]_o$ was evoked by light stimulation in slices prepared from Slc6a3$^{IRES\text{-}Cre}$ mice expressing ChR2, DA axons in striatum were activated by TTL-driven (Multi Channel Stimulus II, Multi Channel Systems) brief pulses (2 ms) of blue light (470 nm; 5 mWmm^{-2}; OptoLED; Cairn Research), which illuminated the field of view (2.2 mm, x10 water-immersion objective). Epifluorescence used to visualize ChR2-eYFP expression was used sparingly to minimize ChR2 activation before recordings

Electrophysiology. Individual slices were hemisected and transferred to a recording chamber and superfused at ~3.0 mL/min with aCSF at 31-33 °C. Cells were visualized through a X40 water-immersion objective with differential interference contrast optics. All whole-cell experiments were recorded using borosilicate glass pipettes with resistances in the 3 – 5 MΩ range and were pulled on a Flaming- Brown micropipette puller (P-1000, Sutter Instruments). Whole-cell voltage-clamp electrophysiology recordings were made from spiny projection neurons (SPNs; identified by their membrane properties (Gertler et al., 2008; Planert et al., 2013)) in the DLS or NAcC. SPNs were voltage-clamped at -70 mV using a MultiClamp 700B amplifier (Molecular Devices) and with pipettes filled with a CsCl-based internal solution (in mM 120 CsCl, 15 $CsMeSO_3$, 8 NaCl, 0.5 EGTA, 10 HEPES, 2 Mg-ATP, 0.3 Na-GTP, 5 QX-314; pH 7.3 adjusted with CsOH; osmolarity ranging from 305 - 310 mOsmkg^{-1}). The recording perfusate always contained NBQX (5 µM) and APV (50 µM) to block AMPA and NMDA receptor-mediated inward currents. Errors due to the voltage drop across the series resistance (<20 MΩ) were left uncompensated and membrane potentials were corrected for a ~5 mV liquid junction potential. Cells were discarded from analysis if if series resistance varied by more than 15% or increased over 25 MΩ.

To record tonic $GABA_A$ currents, SPNs voltage-clamped at -70 mV were recorded in gap-free mode. Cells were allowed to stabilize for 5-10 min before drug manipulations: GAT inhibitors were bath applied for 20 -25 min; picrotoxin (100 µM) for an additional 3-5 min. Recordings of light-evoked GABA currents in SPNs from ChR2-expressing DA axons in slices from Slc6a3$^{IRES\text{-}Cre}$ mice were taken 10 min after break-in, and at 30 s intervals for a duration of 10 min from SPNs voltage-clamped at -70 mV. Under these conditions, $GABA_A$ receptor-mediated currents appear inward as reported previously (Tritsch et al., 2012). TTL-driven (Multi Channel Stimulus II, Multi Channel Systems) brief pulses (2 ms) of blue light (470 nm; 5 mWmm^{-2}; OptoLED; Cairn Research) illuminated the full field of view (2.2 mm, X10 water-immersion objective).

High-performance liquid chromatography. DA content in dorsal striatum was measured by HPLC with electrochemical detection as described previously (Janezic et al., 2013). Tissue punches (2 mm in diameter) were taken from dorsal striatum in two brain slices per animal, snap frozen and stored at −80 °C in 200 µL 0.1 M $HClO_4$. On the day of analysis, samples were thawed on ice, homogenized, and centrifuged at 15,000 g for 15 min at 4 °C. The supernatant was analysed for DA content. Analytes were separated using a 4.6 × 250 mm Microsorb C18 reverse-phase column (Varian or Agilent) and detected using a Decade II SDS electrochemical detector with a Glassy carbon working electrode (Antec Leyden) set at + 0.7 V with respect to a Ag/AgCl reference electrode. The mobile phase consisted of 13% methanol (vol/vol), 0.12 M NaH_2PO_4, 0.5–4.0 mM octenyl succinic anhydride (OSA), and 0.8 mM EDTA (pH 4.4–4.6), and the flow rate was fixed at 1 mL/min.

Western blot. Mouse brains were extracted and sliced using the procedures outlined above. One 1.2 mm thick coronal slice containing striatum was prepared from each brain and one tissue punch (2 mm in diameter) of dorsal striatum taken per hemisphere. Striatal tissue samples were snap-frozen and stored at at −80 °C. For analysis, striatal tissue was defrosted on ice, homogenized in RIPA Lysis and Extraction Buffer (Sigma) containing 150 mM NaCl, 1.0% IGEPAL, 0.5% sodium deoxycholate, 0.1% SDS, 50 mM Tris, pH 8.0, with Complete-Mini Protease Inhibitor and PhosStop (Roche), using a Tissue Tearor (Biospec Products, Inc), and soluble fraction isolated by microcentrifugation at 15,000 g for 15 min at 4°C. Total protein content was quantified using a BCA Protein Assay Kit (Thermo Scientific) and equal amounts of total protein were loaded onto 4 – 15% Tris-Glycine gels (BioRad). Following electrophoresis (200 V for ~45 min), proteins were transferred onto polyvinylidene fluoride membranes (BioRad). Blots were probed overnight at 4°C with 1:1,000 rabbit anti-GABA transporter 1 (Synaptic Systems, 274102) or 1:1,000 rabbit anti-GABA transporter 3 (Abcam, AB181783). Blots were incubated with HRP-conjugated secondary anitbodies at 1:3,000 for 1 h at room temperature and bands developed using ECL Prime Western Blotting Detection Reagent (GE Healthcare). Blots were subsequently incubated with 1:20,000 HRP-conjugated β-actin (Abcam, AB49900) for 1 h at room temperature and bands developed as above. Visualization and imaging of blots was performed with a ChemiDoc Imaging System (BioRad) and bands quantified using Image Lab Software (BioRad). Protein concentration for GAT-1 and GAT-3 were normalized to β-actin.

Indirect immunofluorescence. Adult mice were anaesthetized with an overdose of pentobarbital and transcardially perfused with 20-50 mL of phosphate-buffered saline (PBS), followed by 30-100 mL of 4% paraformaldehyde (PFA) in 0.1 M phosphate buffer, pH 7.4. Brains were removed and post-fixed overnight in 4% PFA. Brains were embedded in agar (3-4%) and coronal sections (50 µm) were cut on a vibrating microtome (Leica VT1000S) and collected in a 1 in 4 series. Sections were stored in PBS with 0.05% sodium azide. Upon processing, sections were washed in PBS and then blocked for 1h in a solution of PBS TritonX (0.3%) with sodium azide (0.02%; PBS-Tx) containing 10% normal donkey serum (NDS). Sections were then incubated in primary antibodies overnight in PBS-Tx with 2% NDS at 4°C. Primary antibodies: rabbit anti-TH

(1:2,000, Sigma-Aldrich, ab112); rabbit anti-GAT1 (1:1,000, Synaptic Systems, 274102); rabbit anti-GAT3 (1:250, Millipore/Chemicon, AB1574); guinea pig anti-S100β (1:2,000, Synaptic Systems, 287004); rat anti-GFP that also recognizes eYFP (1:1,000, Nacalai Tesque, 04404-84); and guinea-pig anti-parvalbumin (1:1,000, Synaptic Systems, 195004). Sections were then incubated in species-appropriate fluorescent secondary antibodies with minimal cross-reactivity overnight in PBS-Tx at room temperature (Donkey anti-Rabbit AlexaFluor 488, 1:1,000, Invitrogen, A21206; Donkey anti-Rabbit Cy3, 1:1,000, Jackson ImmunoResearch, 711-165-152; Donkey anti-Guinea Pig AlexaFluor 488, 1:1,000, Jackson ImmunoResearch, 706-545-148; Donkey anti-Rat AlexaFluor 488, 1:1,000, Jackson ImmunoResearch, 712-545-153). Sections were washed in PBS and then mounted on glass slides and cover-slipped using Vectashield (Vector Labs). Coverslips were sealed using nail varnish and stored at 4°C. To verify the specificity of ChR2-EYFP expression in TH-positive structures in Slc6a3$^{IRES\text{-}Cre}$ mice, mounted sections were imaged with an Olympus BX41 microscope with Olympus UC30 camera and filters for appropriate excitation and emission wave lengths (Olympus Medical).

Confocal imaging and image analysis. Confocal images were acquired with an LSM880/Axio.Imager Z2 (Zeiss) and Image J was used for image analysis. For whole striatum analysis of GAT1 or GAT3, the X10 (NA = 0.45) objective was used and all imaging settings (laser %, pinhole/optical section, pixel size, gain, and scanning speed) were kept constant between animals. For the quantification of fluorescence (mean grey values), 4 sections in the rostro-caudal plane were imaged at approximately the following distances rostral of Bregma; +1.3mm, +1.0mm, +0.6mm, and +0.25mm (see Supplementary Figure S4). A region of interest (ROI) of 300 µm x 300 µm was overlaid over the DLS and the ventral CPu (vCPu); and an ROI of 200 µm X 200 µm was overlaid on NAcC and the NAcS, for both hemispheres. Values for NAcC and NAcS were taken from the 2 most rostral sections (see Supplementary Figure 4). Mean grey values from the areas of interest were normalized to the median grey value for each hemisphere (n = 12 hemispheres from 6 animals). For examination of co-localization a X63 objective was used (NA = 1.46); Z-stacks were taken with the pinhole set to 1 Airy Unit (optical section = 0.7µm) with a z-stack interval of 0.35 µm. In order to assess co-localization ZEN (blue edition v.2.3; Zeiss) software was used. For S100β, PV+ axons (eYFP in PV-Cre mice) or dopaminergic axons (eYFP in *Slc6a3*$^{IRES\text{-}Cre}$ mice) and GAT1/3 co-localization, stacks from 2 striatal regions and 2 NAcC regions in at least one section were examined per animal (n = 3 per marker).

Drugs. (S)-SNAP5114 (SNAP, 50 µM), (±)-nipecotic acid (NPA, 1.5 mM), γ-aminobutyric acid (GABA, 2 mM) and picrotoxin (100 µM) were obtained from Sigma Aldrich. Dihydro-β-erythroidine hydrobromide (DHβE, 1 µM), (+)-bicuculline (10 µM) and tetrodotoxin (1 µM) were obtained from Tocris Bioscience. DL-2-Amino-5-phosphonovaleric acid (AP5, 50 µM), disulfiram (10 µM) and SKF-89976A hydrochloride (SKF, 20 µM) were obtained from Santa Cruz Biotechnology. NBQX disodium salt (NBQX, 5 µM) and CGP 55845 hydrochloride (CGP, 4 µM) were obtained from Abcam. Fluorocitrate was prepared as previously described (Paulsen et al., 1987). In brief, D,L-fluorocitric acid Ba_3 salt (Sigma Aldrich) was dissolved in 0.1 M HCl, the Ba^{2+} precipitated

with 0.1 M Na_2S0_4 and then centrifuged at 1,000 g for 5 min. Supernatant containing fluorocitrate was used at a final concentration of 200 µM for experimentation. All drugs were dissolved in distilled water or dimethyl sulfoxide (DMSO) to make stock aliquots at 1,000–10,000 × final concentrations and stored at −20 °C. Stock aliquots were diluted with aCSF to final concentration immediately before use.

Data acquisition and analysis. FSCV data were digitized at 50 kHz using a Digidata 1550A digitizer (Molecular Devices). Data were acquired and analyzed using Axoscope 11.0 (Molecular Devices) and locally written VBA scripts. For drug effects, peak $[DA]_o$ was averaged over 4 stimulations once peak $[DA]_o$ had re-stabilized post-drug application and compared to time-matched data from drug-free controls, unless otherwise stated. Electrically evoked $[DA]_o$ in slices pre-incubated in fluorocitrate (200 µM) exhibited ongoing run-down across repeated 1p stimulations (n = 5 experiments/3 mice; data not shown) and therefore we used an alternative stimulation paradigm to compare a large number of dorsal striatal recording sites in slices pre-treated with fluorocitrate versus control conditions to minimize run-down. FSCV data are normalized to pre-drug conditions for clarity and for comparisons between regions. For experiments involving multiple pulse protocols, each stimulation type was repeated in triplicate, interspersed with 1p stimulations, and then averaged and normalized to 1p stimulations at each recording site, as previously (Lopes et al., 2018; Threlfell et al., 2012).

Membrane currents from voltage-clamp electrophysiology experiments were amplified and low-pass filtered at 5 kHz using a MultiClamp 700B amplifier (Molecular Devices), digitized at 10 kHz and acquired using a Digidata 1550A digitizer (Molecular Devices). Peak amplitude, onset latency, peak latency, 10-90% rise time and decay time were measured from an average of 3 replicate traces recorded before and after drug wash on conditions using Clampfit 10.4.1.4 software (Molecular Devices).

For all experiments, data were collected from a minimum of 3 animals. Data were compared for statistical significance using Prism 7 (Graph Pad) with the following statistical tests (as indicated in the text, and two-tailed): un-paired t-tests, paired t-tests, two-way repeated-measures ANOVA followed by Sidak's multiple comparisons, and where the data were not normally distributed, Mann-Whitney U tests, Kruskal-Wallis ANOVA followed by Dunn's Multiple Comparisons, Friedman's ANOVA on Ranks and Student-Newman-Keuls multiple comparisons and for comparing cumulative distributions, Komogorov-Smirnov tests. p values smaller than 0.05 were considered statistically significant, adjusted for multiple comparisons.

Acknowledgements

This work is supported by grants from Parkinson's UK (G-1504, and Monument Trust Discovery Award J-1403), a Clarendon Fund Studentship awarded to B.M.R. and a Fundação para a Ciência e a Tecnologia studentship awarded to E.F.L. N.M.D. and P.J.M. were supported by the UK Medical Research Council (Award MC_UU_12024/2 to P.J.M.) and the Wellcome Trust (Investigator Award 101821 to P.J.M.). We thank Ben Micklem and Lisa Conyers for their assistance with anatomical work, Milena Cioroch for technical expertise in maintaining transgenic mouse colonies, and members of the Cragg laboratory for discussions throughout the course of this study. We thank Drs Yoland Smith and Jean-Francois Pare for GAT antibody recommendations.

Author contributions

B.M.R. and S.J.C. conceived and designed the research, and wrote the manuscript with input from all other authors. B.M.R. performed the majority of experiments and analysis of data. N.M.D. and P.J.M. collected, analysed and interpreted anatomical confocal imaging data. K.R.B, E.F.L., S.T. and R.E.S. assisted with the collection, analysis and interpretation of voltammetry data. N.C.-R. and N.B.-V. provided expertise and assistance with western blot experiments. R.W.-M. conceived of and provided the SNCA-OVX model and assisted in interpretation of data.

Competing financial interests

The authors declare no competing financial interests.

REFERENCES

Ade, K.K., Janssen, M.J., Ortinski, P.I., and Vicini, S. (2008). Differential Tonic GABA Conductances in Striatal Medium Spiny Neurons. J. Neurosci. *28*, 1185–1197.

Augood, S.J., Herbison, A.E., and Emson, P.C. (1995). Localization of GAT-1 GABA transporter mRNA in rat striatum: cellular coexpression with GAD67 mRNA, GAD67 immunoreactivity, and parvalbumin mRNA. J. Neurosci. *15*, 865–874.

Boddum, K., Jensen, T.P., Magloire, V., Kristiansen, U., Rusakov, D.A., Pavlov, I., and Walker, M.C. (2016). Astrocytic GABA transporter activity modulates excitatory neurotransmission. Nat. Commun. *7*, 13572.

Bonansco, C., Couve, A., Perea, G., Ferradas, C.A., Roncagliolo, M., and Fuenzalida, M. (2011). Glutamate released spontaneously from astrocytes sets the threshold for synaptic plasticity. Eur. J. Neurosci. *33*, 1483–1492.

Borden, L.A. (1996). GABA transporter heterogeneity: Pharmacology and cellular localization. Neurochem. Int. *29*, 335–356.

Brickley, S.G., and Mody, I. (2012). Extrasynaptic GABAA Receptors: Their Function in the CNS and Implications for Disease. Neuron *73*, 23–34.

Brimblecombe, K.R., Gracie, C.J., Platt, N.J., and Cragg, S.J. (2015). Gating of dopamine transmission by calcium and axonal N-, Q-, T- and L-type voltage-gated calcium channels differs between striatal domains. J. Physiol. *593*, 929–946.

Britt, J.P., and McGehee, D.S. (2008). Presynaptic Opioid and Nicotinic Receptor Modulation of Dopamine Overflow in the Nucleus Accumbens. J. Neurosci. *28*, 1672–1681.

Cepeda, C., Galvan, L., Holley, S.M., Rao, S.P., Andre, V.M., Botelho, E.P., Chen, J.Y., Watson, J.B., Deisseroth, K., and Levine, M.S. (2013). Multiple Sources of Striatal Inhibition Are Differentially Affected in Huntington's Disease Mouse Models. J. Neurosci. *33*, 7393–7406.

Chai, H., Diaz-Castro, B., Shigetomi, E., Monte, E., Octeau, J.C., Yu, X., Cohn, W., Rajendran, P.S., Vondriska, T.M., Whitelegge, J.P., et al. (2017). Neural Circuit-Specialized Astrocytes: Transcriptomic, Proteomic, Morphological, and Functional Evidence. Neuron *95*, 531-549.e9.

Charara, A., Heilman, C., Levey, A.., and Smith, Y. (1999). Pre- and postsynaptic localization of GABAB receptors in the basal ganglia in monkeys. Neuroscience *95*, 127–140.

Chazalon, M., Paredes-Rodriguez, E., Morin, S., Martinez, A., Cristóvão-Ferreira, S., Vaz, S., Sebastiao, A., Panatier, A., Boué-Grabot, E., Miguelez, C., et al. (2018). GAT-3 Dysfunction Generates Tonic Inhibition in External Globus Pallidus Neurons in Parkinsonian Rodents. Cell Rep. *23*, 1678–1690.

Dodson, P.D., Dreyer, J.K., Jennings, K.A., Syed, E.C.J., Wade-Martins, R., Cragg, S.J., Bolam, J.P., and Magill, P.J. (2016). Representation of spontaneous movement by dopaminergic neurons is cell-type selective and disrupted in parkinsonism. Proc. Natl. Acad. Sci. U. S. A. *113*, E2180-8.

Durkin, M.M., Smith, K.E., Borden, L.A., Weinshank, R.L., Branchek, T.A., and Gustafson, E.L. (1995). Localization of messenger RNAs encoding three GABA transporters in rat brain: an in situ hybridization study. Mol. Brain Res. *33*, 7–21.

Exley, R., and Cragg, S.J. (2008). Presynaptic nicotinic receptors: A dynamic and diverse cholinergic filter of striatal dopamine neurotransmission. In British Journal of Pharmacology, (John Wiley & Sons, Ltd (10.1111)), pp. S283–S297.

Farrant, M., and Nusser, Z. (2005). Variations on an inhibitory theme: phasic and tonic activation of GABAA receptors. Nat. Rev. Neurosci. *6*, 215–229.

Ficková, M., Dahmen, N., Fehr, C., and Hiemke, C. (1999). Quantitation of GABA transporter 3 (GAT3) mRNA in rat brain by competitive RT-PCR. Brain Res. Protoc. *4*, 341–350.

Gertler, T.S., Chan, C.S., and Surmeier, D.J. (2008). Dichotomous Anatomical Properties of Adult Striatal Medium Spiny Neurons. J. Neurosci. *28*, 10814–10824.

Gokce, O., Neff, N.F., Fuccillo, M. V., Südhof, T.C., Treutlein, B., Quake, S.R., Malenka, R.C., Stanley, G.M., Rothwell, P.E., and Camp, J.G. (2016). Cellular Taxonomy of the Mouse Striatum as Revealed by Single-Cell

RNA-Seq. Cell Rep. *16*, 1126–1137.

Goubard, V., Fino, E., and Venance, L. (2011). Contribution of astrocytic glutamate and GABA uptake to corticostriatal information processing. J. Physiol. *589*, 2301–2319.

Janezic, S., Threlfell, S., Dodson, P.D., Dowie, M.J., Taylor, T.N., Potgieter, D., Parkkinen, L., Senior, S.L., Anwar, S., Ryan, B., et al. (2013). Deficits in dopaminergic transmission precede neuron loss and dysfunction in a new Parkinson model. Proc. Natl. Acad. Sci. *110*, E4016–E4025.

Jennings, K.A., Platt, N.J., and Cragg, S.J. (2015). The impact of a parkinsonian lesion on dynamic striatal dopamine transmission depends on nicotinic receptor activation. Neurobiol. Dis. *82*, 262–268.

Jin, X.-T., Galvan, A., Wichmann, T., and Smith, Y. (2011). Localization and Function of GABA Transporters GAT-1 and GAT-3 in the Basal Ganglia. Front. Syst. Neurosci. *5*, 1–10.

Kaeser, P.S., and Regehr, W.G. (2013). Molecular Mechanisms for Synchronous, Asynchronous, and Spontaneous Neurotransmitter Release. Annu. Rev. Physiol. *76*, 333–363.

Kim, J.I., Ganesan, S., Luo, S.X., Wu, Y.W., Park, E., Huang, E.J., Chen, L., and Ding, J.B. (2015). Aldehyde dehydrogenase 1a1 mediates a GABA synthesis pathway in midbrain dopaminergic neurons. Science (80-.). *350*, 102–106.

Kirmse, K., Dvorzhak, A., Kirischuk, S., and Grantyn, R. (2008). GABA transporter 1 tunes GABAergic synaptic transmission at output neurons of the mouse neostriatum. J. Physiol. *586*, 5665–5678.

Kirmse, K., Kirischuk, S., and Grantyn, R. (2009). Role of GABA transporter 3 in GABAergic synaptic transmission at striatal output neurons. Synapse *63*, 921–929.

Li, G., Shao, C., Chen, Q., Wang, Q., and Yang, K. (2017). Accumulated GABA activates presynaptic GABAB receptors and inhibits both excitatory and inhibitory synaptic transmission in rat midbrain periaqueductal gray. Neuroreport *28*, 313–318.

Liu, J., Zhou, Z., Hodgkinson, C.A., Yuan, Q., Shen, P.-H., Mulligan, C.J., Wang, A., Gray, R.R., Roy, A., Virkkunen, M., et al. (2011). Haplotype-Based Study of the Association of Alcohol-Metabolizing Genes With Alcohol Dependence in Four Independent Populations. Alcohol. Clin. Exp. Res. *35*, 304–316.

Lopes, E.F., Roberts, B.M., Siddorn, R.E., Clements, M.A., and Cragg, S.J. (2018). Inhibition of nigrostriatal dopamine release by striatal GABAA and GABAB receptors. J. Neurosci. 2028–18.

Lozovaya, N., Eftekhari, S., Cloarec, R., Gouty-Colomer, L.A., Dufour, A., Riffault, B., Billon-Grand, M., Pons-Bennaceur, A., Oumar, N., Burnashev, N., et al. (2018). GABAergic inhibition in dual-transmission cholinergic and GABAergic striatal interneurons is abolished in Parkinson disease. Nat. Commun. *9*, 1422.

Matsuda, W., Furuta, T., Nakamura, K.C., Hioki, H., Fujiyama, F., Arai, R., and Kaneko, T. (2009). Single Nigrostriatal Dopaminergic Neurons Form Widely Spread and Highly Dense Axonal Arborizations in the Neostriatum. J. Neurosci. *29*, 444–453.

Ng, C.H., Wang, X.S., and Ong, W.Y. (2000). A light and electron microscopic study of the GABA transporter GAT-3 in the monkey basal ganglia and brainstem. J. Neurocytol. *29*, 595–603.

Oorschot, D.E. (1996). Total number of neurons in the neostriatal, pallidal, subthalamic, and substantia nigral nuclei of the rat basal ganglia: A stereological study using the cavalieri and optical disector methods. J. Comp. Neurol. *366*, 580–599.

Paulsen, R.E., Contestabile, A., Villani, L., and Fonnum, F. (1987). An In Vivo Model for Studying Function of Brain Tissue Temporarily Devoid of Glial Cell Metabolism: The Use of Fluorocitrate. J. Neurochem. *48*, 1377–1385.

Pitman, K.A., Puil, E., and Borgland, S.L. (2014). GABAB modulation of dopamine release in the nucleus accumbens core. Eur. J. Neurosci. *40*, 3472–3480.

Planert, H., Berger, T.K., and Silberberg, G. (2013). Membrane Properties of Striatal Direct and Indirect Pathway Neurons in Mouse and Rat Slices and Their Modulation by Dopamine. PLoS One *8*, e57054.

Rice, M.E., and Cragg, S.J. (2004). Nicotine amplifies reward-related dopamine signals in striatum. Nat. Neurosci. *7*, 583–584.

Santhakumar, V., Jones, R.T., and Mody, I. (2010). Developmental regulation and neuroprotective effects of striatal tonic GABAA currents. Neuroscience *167*, 644–655.

Schmitz, Y., Schmauss, C., and Sulzer, D. (2002). Altered Dopamine Release and Uptake Kinetics in Mice Lacking D 2 Receptors. J. Neurosci. *22*, 8002–8009.

Schmitz, Y., Benoit-Marand, M., Gonon, F., and Sulzer, D. (2003). Presynaptic regulation of dopaminergic neurotransmission. J. Neurochem. *87*, 273–289.

Sherva, R., Rice, J.P., Neuman, R.J., Rochberg, N., Saccone, N.L., and Bierut, L.J. (2009). Associations and Interactions Between SNPs in the Alcohol Metabolizing Genes and Alcoholism Phenotypes in European Americans. Alcohol. Clin. Exp. Res. *33*, 848–857.

Shin, J.H., Adrover, M.F., and Alvarez, V.A. (2017). Distinctive Modulation of Dopamine Release in the Nucleus Accumbens Shell Mediated by Dopamine and Acetylcholine Receptors. J. Neurosci. *37*, 11166–11180.

Sloan, M., Alegre-Abarrategui, J., Potgieter, D., Kaufmann, A.-K., Exley, R., Deltheil, T., Threlfell, S., Connor-Robson, N., Brimblecombe, K., Wallings, R., et al. (2016). *LRRK2* BAC transgenic rats develop progressive, L-DOPA-responsive motor impairment, and deficits in dopamine circuit function. Hum. Mol. Genet. *25*, 951–963.

Sulzer, D., Cragg, S.J., and Rice, M.E. (2016). Striatal dopamine neurotransmission: Regulation of release and uptake. Basal Ganglia.

Taylor, T.N., Potgieter, D., Anwar, S., Senior, S.L., Janezic, S., Threlfell, S., Ryan, B., Parkkinen, L., Deltheil, T., Cioroch, M., et al. (2014). Region-specific deficits in dopamine, but not norepinephrine, signaling in a novel A30P α-synuclein BAC transgenic mouse. Neurobiol. Dis. *62*, 193–207.

Threlfell, S., and Cragg, S.J. (2011). Dopamine Signaling in Dorsal Versus Ventral Striatum: The Dynamic Role of Cholinergic Interneurons. Front. Syst. Neurosci. *5*, 11.

Threlfell, S., Clements, M.A., Khodai, T., Pienaar, I.S., Exley, R., Wess, J., and Cragg, S.J. (2010). Striatal Muscarinic Receptors Promote Activity Dependence of Dopamine Transmission via Distinct Receptor Subtypes on Cholinergic Interneurons in Ventral versus Dorsal Striatum.

Threlfell, S., Lalic, T., Platt, N.J., Jennings, K.A., Deisseroth, K., and Cragg, S.J. (2012). Striatal dopamine release is triggered by synchronized activity in cholinergic interneurons. Neuron *75*, 58–64.

Tritsch, N.X., Ding, J.B., and Sabatini, B.L. (2012). Dopaminergic neurons inhibit striatal output through non-canonical release of GABA. Nature *490*, 262–266.

Tritsch, N.X., Oh, W.J., Gu, C., and Sabatini, B.L. (2014). Midbrain dopamine neurons sustain inhibitory transmission using plasma membrane uptake of GABA, not synthesis. Elife *3*, e01936.

Wójtowicz, A.M., Dvorzhak, A., Semtner, M., and Grantyn, R. (2013). Reduced tonic inhibition in striatal output neurons from Huntington mice due to loss of astrocytic GABA release through GAT-3. Front. Neural Circuits *7*, 188.

Yasumi, M., Sato, K., Shimada, S., Nishimura, M., and Tohyama, M. (1997). Regional distribution of GABA transporter 1 (GAT1) mRNA in the rat brain: comparison with glutamic acid decarboxylase67 (GAD67) mRNA localization. Brain Res. Mol. Brain Res. *44*, 205–218.

Yu, X., Taylor, A.M.W., Nagai, J., Golshani, P., Evans, C.J., Coppola, G., and Khakh, B.S. (2018). Reducing Astrocyte Calcium Signaling In Vivo Alters Striatal Microcircuits and Causes Repetitive Behavior. Neuron *99*, 1170-1187.e9.

Zaccara, G., Cincotta, M., Borgheresi, A., and Balestrieri, F. (2004). Adverse motor effects induced by antiepileptic drugs.

Zhang, Y., Chen, K., Sloan, S.A., Bennett, M.L., Scholze, A.R., O'Keeffe, S., Phatnani, H.P., Guarnieri, P., Caneda, C., Ruderisch, N., et al. (2014). An RNA-Sequencing Transcriptome and Splicing Database of Glia, Neurons, and Vascular Cells of the Cerebral Cortex. J. Neurosci. *34*, 11929–11947.

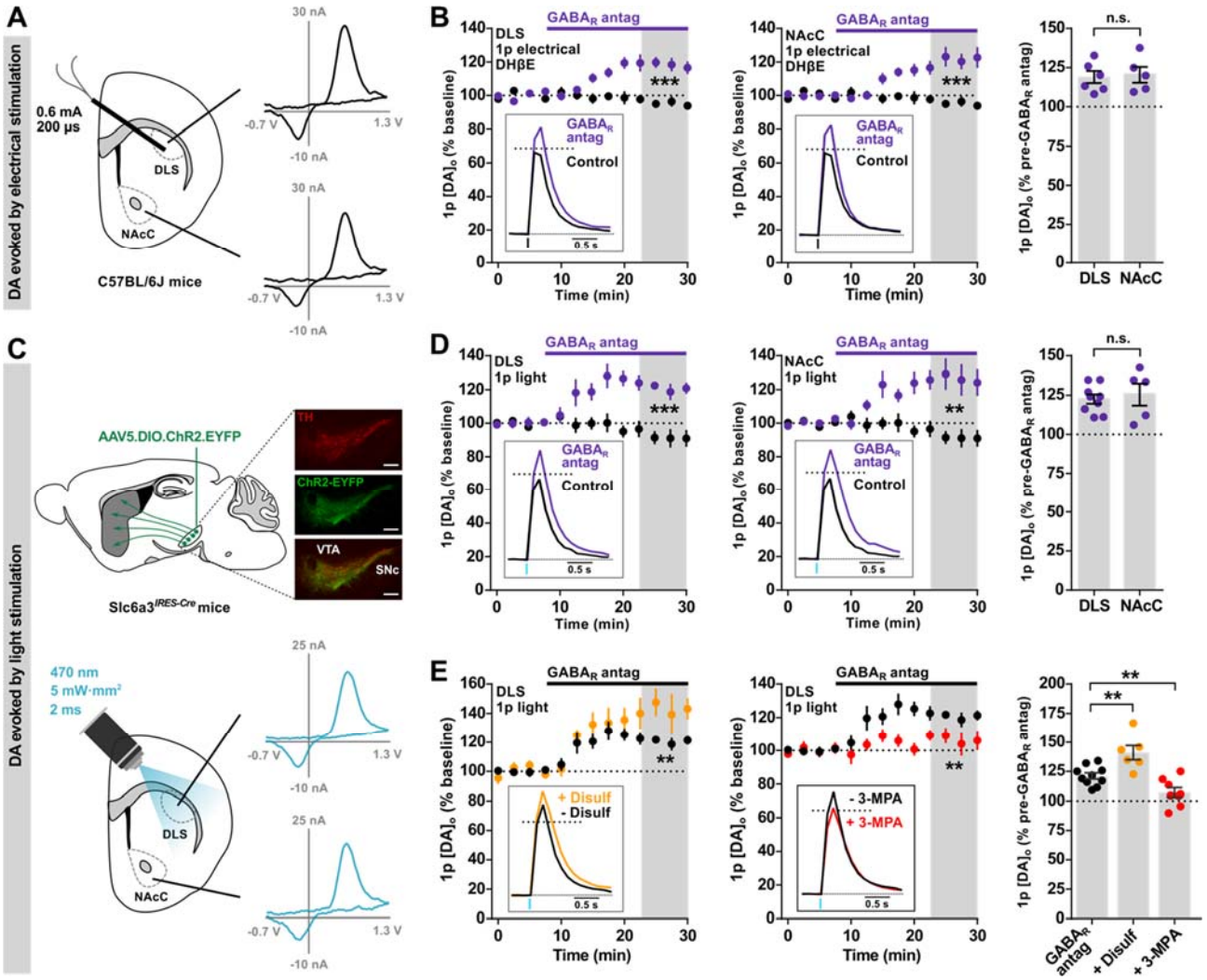

Figure 1. Striatal DA release is under tonic inhibition by a GAD-dependent GABA source.

(**A**,**C**) Schematics representing the experimental configuration and representative voltammograms for (**A**) electrically evoked $[DA]_o$ or (**C**) light-evoked $[DA]_o$, after injection and expression of viral ChR2-eYFP in VTA and SNc (top) in Slc6a3$^{IRES\text{-}Cre}$ mouse. TH (*red*), ChR2-eYFP (*green*). Scale bars in (**C**): 0.25 mm. (**B**,**D**) Mean peak $[DA]_o$ (± SEM) during consecutive recordings evoked by a single electrical (**B**) or light pulse (**D**) (*1p*) in control conditions (*black*, n = 9 experiments/7 mice for electrical, n = 8 experiments/6 mice for light) and with $GABA_A$ and $GABA_B$ receptor antagonists (*solid bar*)(*purple*, *GABA$_R$ antag*), (+)-bicuculline (10 µM) and CGP 55845 (4 µM), respectively, recorded in the DLS (*left*, n = 6 experiments/3 mice for electrical, n = 9 experiments/5 mice for light) or NAcC (*middle*, n = 5 experiments/3 mice for electrical, n = 5 experiments/4 mice for light). *Right*, mean peak $[DA]_o$ (± SEM) evoked by 1p following $GABA_R$ antagonism in DLS and NAcC (as % of pre-drug baseline). (**E**) *Left,* Mean peak $[DA]_o$ (± SEM) during consecutive recordings evoked by 1p light during application of $GABA_R$ antagonists in the absence (*black*, n = 10 experiments/7 mice) or the presence of ALDH inhibitor disulfiram (10 µM) (*orange*, n = 6 experiments/5 mice) or GAD inhibitor 3-MPA (5000 µM) (*red*, n = 7 experiments/5 mice). *Right*, Mean peak $[DA]_o$ (± SEM) in DLS following $GABA_R$ antagonism in the absence or the presence of 3-MPA (expressed as a % of pre-drug baseline). Statistical significance was assessed by Mann-Whitney tests. $^{**}P < 0.01$, $^{***}P < 0.0001$, n.s. not significant. Data are normalized to mean of 4 time points prior to GABA antagonist application (*dotted line*); last 4 time points (*gray shaded region*) are used for statistical comparisons. *Inset*, mean transients of $DA]_o$ observed at each stimulus normalized to pre-drug baselines. DHβE (1 µM) was present for experiments with electrical stimuli.

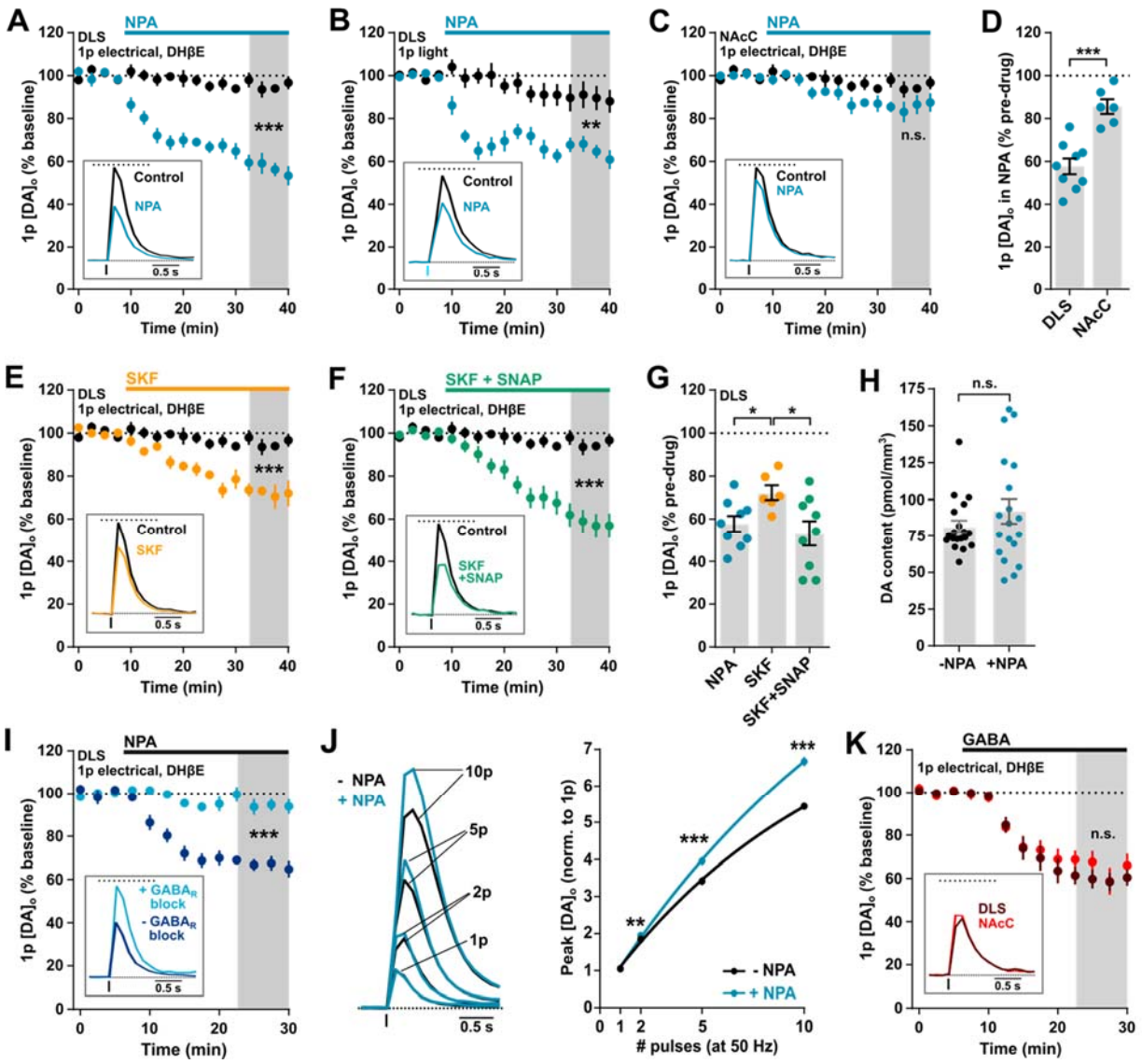

Figure 2. GAT inhibition attenuates DA release in DLS, but not NAcC, by increasing GABA receptor tone.

(**A-C,E-F**) Mean peak $[DA]_o$ (± SEM) during consecutive recordings evoked by a single electrical (**A**,**C**,**E**,**F**,**K**) or light pulse (**B**) in DLS (**A**,**B**,**E**,**F**,**K**) or NAcC (**C**) in control conditions (*black*, n = 9 experiments/7 mice for electrical, n = 8 experiments/6 mice for light) or with GAT inhibitor NPA (1.5 mM) (**A,** *blue*, n = 9 experiments/5 mice; **B,** n = 9 experiments/5 mice; **C,** n = 6 experiments/4 mice), the GAT-1 specific inhibitor SKF89976A (20 μM) (**E,** *orange*, n = 6 experiments/4 mice), or the combined bath application of SKF89976A and the GAT-3 specific inhibitor SNAP5114 (50 μM) (**F,** *green*, n = 9 experiments/5 mice). (**D**,**G**) Mean peak $[DA]_o$ (± SEM) evoked by 1p following GAT inhibition (expressed as a % of pre-drug baseline). (**H**) Mean DA content (± SEM) of dorsal striatum incubated in vehicle-treated control conditions (*black*, n = 19 punches/5 mice) or NPA (1.5 mM) (*blue*, n = 19 punches/5 mice). (**I**) Mean peak $[DA]_o$ (± SEM) during consecutive recordings evoked by a 1 electrical pulse in DLS during application of NPA (1.5 mM) in the absence (*dark blue*, n = 9 experiments/5 mice) or presence (*light blue*, n = 5 experiments/4 mice) of $GABA_A$ (picrotoxin, 100 μM) and $GABA_B$ (CGP 55845, 4 μM) receptor antagonists. (**J**) *Left*, Mean profiles and *right,* mean peak values of $[DA]_o$ evoked by 50 Hz electrical pulses in DLS normalized to 1p in the absence (*black*, control, n = 8 experiments/5 mice) or presence of NPA (1.5 mM) (*blue*, n = 8 experiments/5 mice). *Right*, Sigmoidal curve fits (R^2 = 0.98). (**K**) Mean peak $[DA]_o$ (± SEM) with application of GABA (2 mM) in DLS (*dark red*, n = 6 experiments/4 mice) and NAcC (*light red*, n = 5 experiments/4 mice). Mann-Whitney tests (A-F, H, I, K), Kruskal-Wallis test and Dunn's multiple comparisons (G), two-way RM ANOVA and Sidak's multiple comparisons (J). **P* < 0.05, ***P* < 0.01, ****P* < 0.0001, n.s. not significant. Data are normalized to first 4 time points (*dotted line*); last 4 time points (*gray shaded region*) are used for statistical comparisons. Insets, mean transients of $[DA]_o$ (normalized to pre-drug baselines). DHβE (1 μM) present throughout experiments with electrical stimuli.

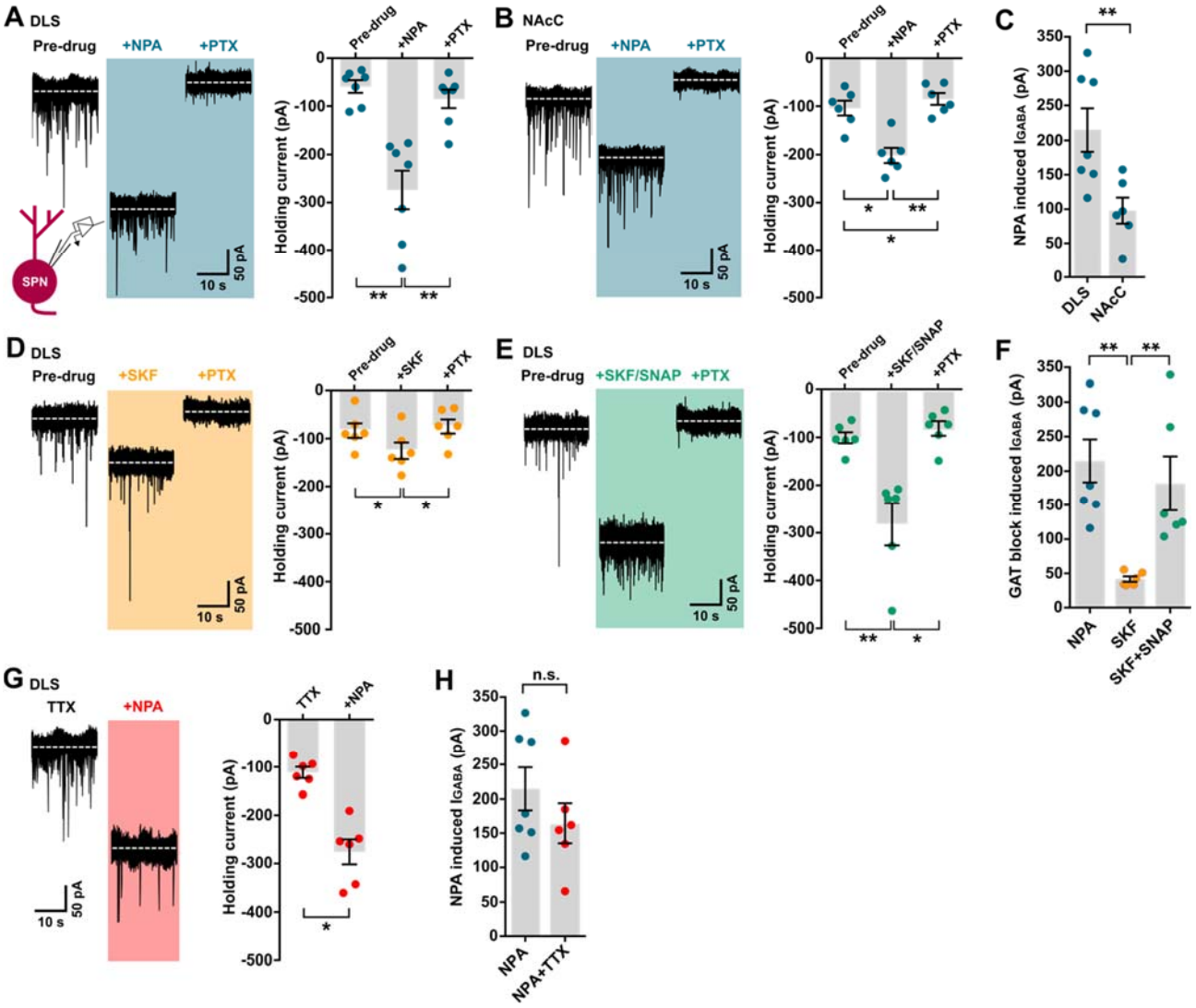

Figure 3. Tonic GABA currents in striatal spiny projection neurons (SPNs) are augmented by GAT inhibition.
(**A-B,D-E,G**) *Left*, representative continuous whole-cell recordings from SPNs in DLS (A,D,E,G) or NAcC (B), voltage-clamped at -70 mV in the presence of ionotropic glutamate receptor antagonists NBQX (5 μM) and D-AP5 (50 μM), before and during bath application of (A-B) GAT inhibitor NPA (*blue*, 1.5 mM, n = 7 cells/5 mice for DLS in A, n = 6 cells/3 mice for NAcC in B), (D) GAT-1 specific inhibitor SKF89976A (*orange*, 20 μM, n = 6 cells/3 mice), (E) the combined application of SKF89976A and GAT-3 specific inhibitor SNAP5114 (*green*, 50 μM, n = 6 cells/4 mice), or (G) NPA in the presence of TTX (1 μM) (*red*, n = 6 cells/3 mice). GAT inhibitors increase the extracellular $GABA_A$-mediated inward current, revealed by a shift in the holding current, and is reversed upon application of $GABA_A$ receptor antagonist picrotoxin (PTX, 100 μM). *Right*, mean (± SEM) holding current in pA recorded in SPNs in control conditions, upon addition of GAT inhibitors and then PTX. (**C**,**F**,**H**) Mean (± SEM) tonic $GABA_A$-receptor-mediated currents induced by GAT inhibition recorded from SPNs, calculated by subtracting pre-drug holding current from GAT block-induced holding current. Friedman's ANOVA on Ranks and Student-Newman-Keuls multiple comparisons (A,B,D,E), Mann-Whitney tests (C,H), Kruskal-Wallis test and Dunn's multiple comparisons (F), Wilcoxon signed-rank test (G) **P* < 0.05, ***P* < 0.01., n.s. not significant.

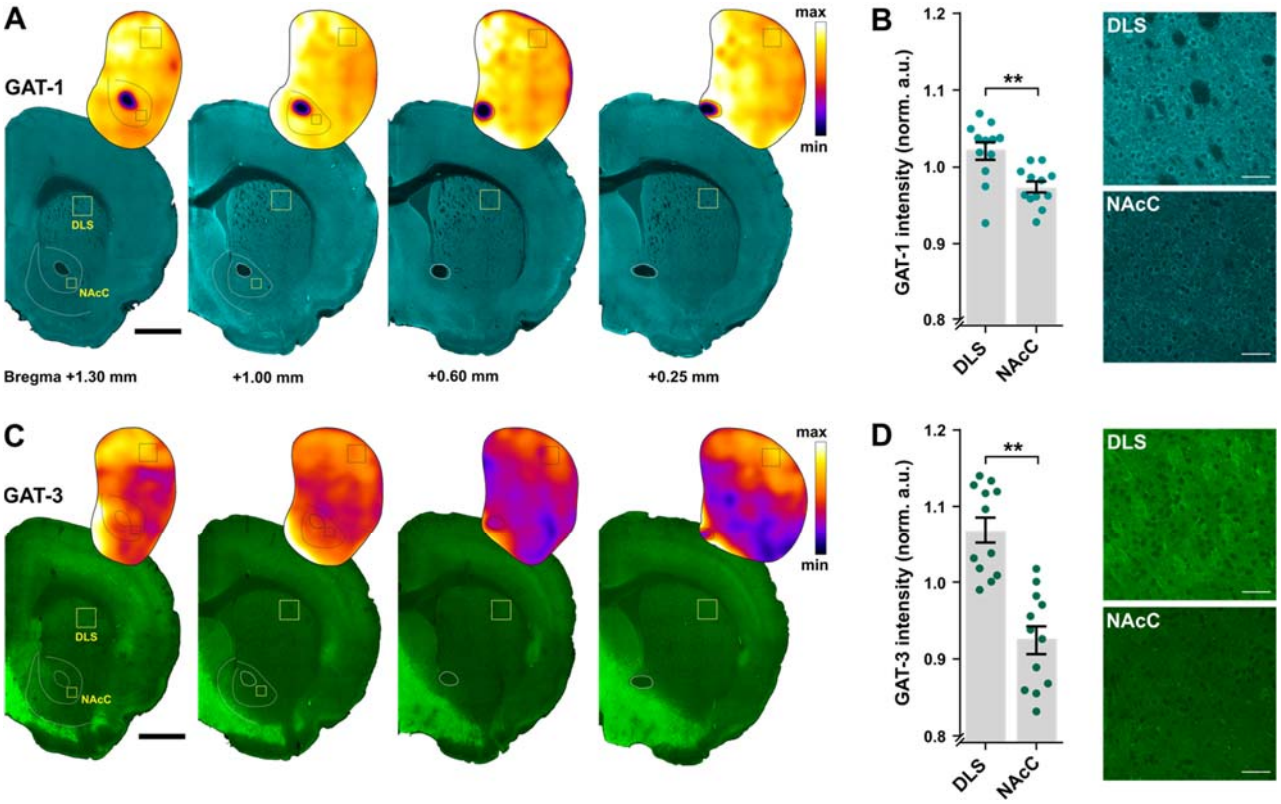

Figure 4. Enrichment of GAT-1 and GAT-3 expression in the DLS versus NAcC.

(**A**,**C**) Representative immunofluorescence signals for GAT-1 (*cyan*, A) and GAT-3 (*green*, C) using confocal microscopy in coronal sections across the rostral-caudal limits containing striatum prepared from an individual C57BL/6J mouse with heat maps for striatal GAT intensity. Boxes indicate representative locations for GAT intensity measurements in the dorsolateral striatum (DLS) and nucleus accumbens core (NAcC). Scale bars: 1 mm. Note enriched GAT-3 in the medial NAc shell (NAcS) contiguous with the medial septal nucleus and enriched GAT-3 expression in the claustrum. (**B**,**D**) *Left*, Mean (± SEM) GAT-1 (B) and GAT-3 (D) intensity in DLS and NAcC normalized to total striatum and averaged across rostral-caudal sites for each hemisphere (n = 12 hemispheres/6 mice for each GAT-1 and GAT-3). *Right*, Representative single plane images of GAT-1 (B) and GAT-3 (D) immunofluorescence from DLS and NAcC; imaging parameters were kept constant across regions. Scale bars: 50 μm. Mann-Whitney tests. $^{**}P < 0.01$.

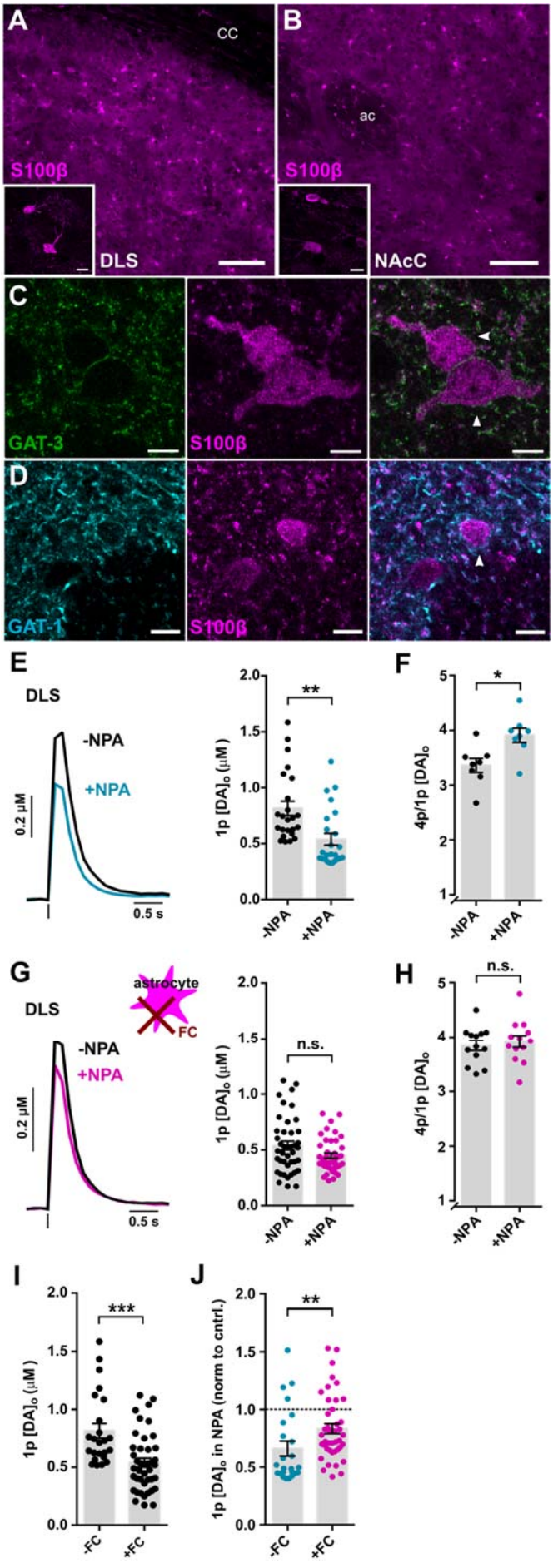

Figure 5. GAT-3 and GAT-1 expressed on striatal astrocytes regulate GABA inhibition of DA release. (**A**-**B**) Striatal immunofluorescence signals for astrocyte marker S100β (*magenta*) in dorsolateral striatum (*DLS*, **A**) and nucleus accumbens core (*NAcC,* **B**). Scale bars: 100 µm, for inset: 10 µm. *cc*: corpus callosum, *ac*: anterior commissure. (**C**-**D**) GAT-3 (*green*, **C**) and GAT-1 (*cyan*, **D**) are expressed on plasma membranes of striatal S100β-expressing astrocytes imaged in DLS (n = 3 animals). Note that localization of GATs on astrocytes (*white arrows*) was more prevalent for GAT-3 than GAT-1. Scale bars: 5 µm. (**E**-**H**) Mean profiles of $[DA]_o$ and mean peak $[DA]_o$ (± SEM) in DLS evoked by 1 electrical pulse (E,G) or 4 pulses normalized to 1p (F,H) in the absence (*black*) and presence of GAT inhibitor NPA (*blue* or *pink*, 1.5 mM) in vehicle-treated control slices (E,F, n = 5 mice) or in slices treated with astrocyte inhibitor fluorocitrate (FC, 200 µM, G,H, n = 7 mice). (I) Mean peak $[DA]_o$ (± SEM) evoked by 1 electrical pulse in the absence of NPA in control slices (-*FC*) and in fluorocitrate-treated slices (+FC) from (E,G). (**J**) Mean peak $[DA]_o$ (± SEM) evoked by 1 electrical pulse in the presence of NPA (1.5 mM) normalized to control conditions in control slices (*blue*) or fluorocitrate-treated slices (*pink*). DHβE (1 µM) present throughout. Mann-Whitney tests (E-J). ***P* < 0.01, *** *P* < 0.001, n.s. not significant.

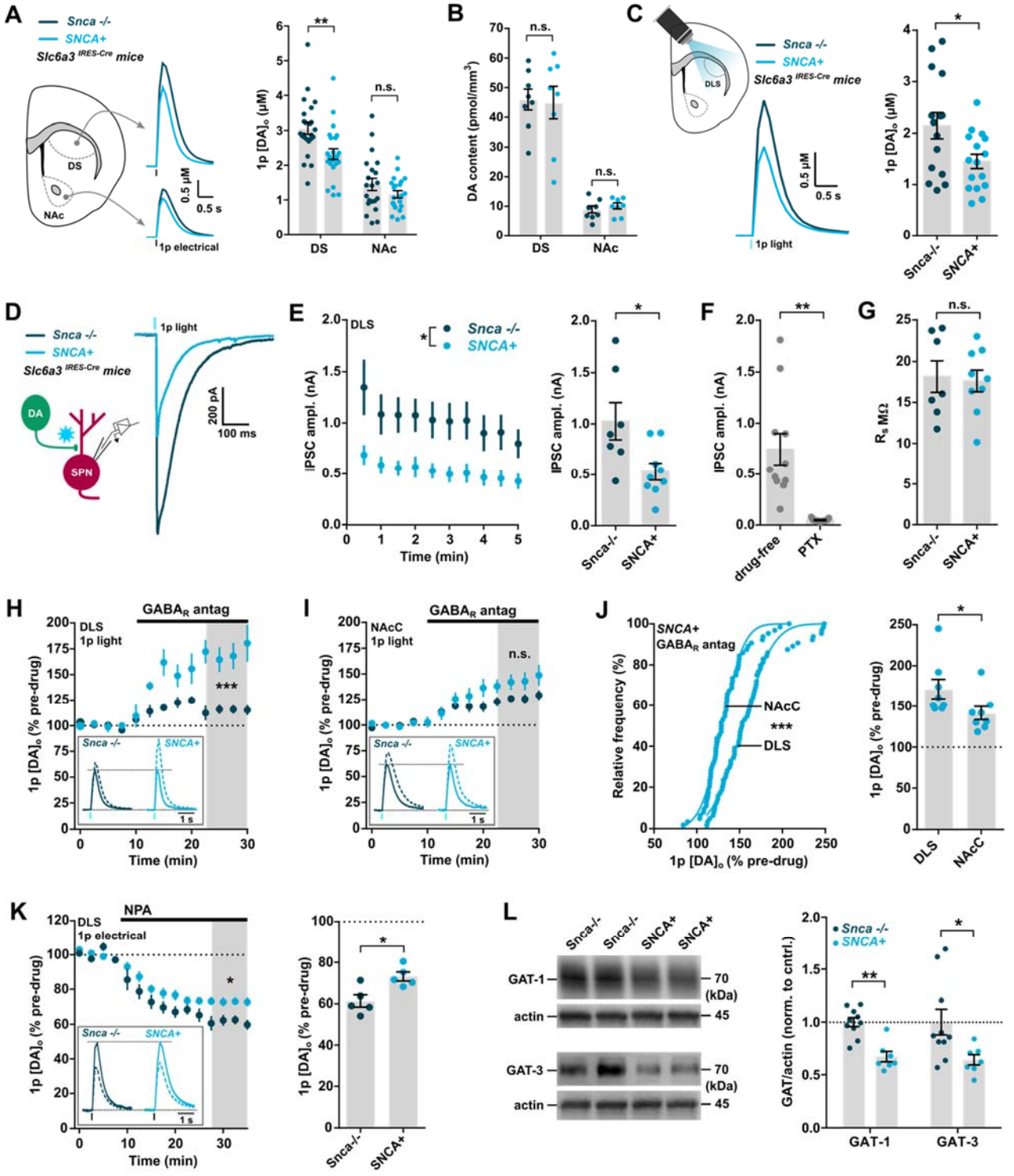

Figure 6. Enhanced tonic inhibition of striatal DA release and reduced co-release of DA and GABA from DA axons in a mouse model of early parkinsonism. (**A**) *Left*, mean $[DA]_o$ profiles vs. time following 1-pulse electrical simulation in dorsal striatum (DS) and nucleus accumbens (NAc) of *SNCA*+ mice (*light blue*) and littermate controls (*Snca-/-*, *dark blue*) at 3-4 months, backcrossed onto an *Slc6a3*$^{IRES\text{-}Cre}$ background. *Right*, Mean (± SEM) 1p-evoked $[DA]_o$ (in µM) from *Left* (n = 24 observations/5 mice per genotype in DS, n = 21 observations/5 mice per genotype in NAc). (**B**) Mean (± SEM) DA content in DS and NAc of *SNCA*+ mice (*light blue*) and littermate controls (*Snca-/-*, *dark blue*) (n = 8 experiments/5 mice per genotype in DS and NAc). (**C**) *Left*, mean $[DA]_o$ profiles vs. time following 1-pulse light simulation in DLS of *SNCA*+ mice (*light blue*) and littermate controls (*Snca-/-*, *dark blue*). *Right*, Mean (± SEM) 1p-evoked $[DA]_o$ (in µM) from *Left* (n = 15 observations/3 mice in Snca-/- mice, n = 16 observations/3 mice in SNCA+ mice). (**D-G**) Mean (± SEM) 1-pulse light-

evoked inhibitory postsynaptic currents (IPSCs) recorded from spiny projection neurons (SPNs) every 30s in the DLS of *SNCA+* mice (*light blue,* n = 9 cells/4 mice) and littermate controls (*Snca-/-*, *dark blue*, n = 7 cells/4 mice), voltage clamped at -70 mV and in the presence of ionotropic glutamate receptor antagonists (NBQX, 5 μM; D-APV, 50 μM). IPSCs in SPNs of both *SNCA+* and *Snca-/-* mice were abolished in the presence of $GABA_A$ receptor antagonist picrotoxin (PTX, 100 μM, **F**) and differences in recorded IPSC amplitude not due to differences in series resistance (R_s) between recordings (**G**). (**H**,**I,K**) Mean peak $[DA]_o$ (± SEM) during consecutive recordings evoked by 1p light (H,I) or electrical pulse (K) in DLS (H,K) or NAcC (I) during applications of antagonists for $GABA_A$ (bicuculline, 10 μM) and $GABA_B$ receptors (CGP 55845, 4 μM) (H,I), or the nonspecific GAT inhibitor NPA (1.5 mM, K) in *Snca-/-* (*dark blue*, $GABA_R$ antagonism: n = 7 experiments/5 mice in DLS, n = 9 experiments/5 mice for NAcC, NPA: n = 5 experiments/4 mice) and *SNCA+* mice (*light blue*, $GABA_R$ antagonism: n = 8 experiments/5 mice for both DLS and NAcC, NPA: n = 5 experiments/4 mice) mice. Data are normalized to first 4 time points (*dotted line*); last 4 time points (*gray shaded region*) are used for statistical comparisons. Insets, mean transients showing release and uptake of $[DA]_o$ in drug condition (*dashed traces*) vs pre-drug condition (*solid traces*), normalized to pre-drug baselines. (**J**) Cumulative frequency plots of individual data points (*left*) and mean (± SEM) per recording site (*right*) from (D,E) for *SNCA+* mice in for DLS and NAcC recordings following $GABA_R$ antagonism. (**L**) Representative Western blots and mean (± SEM) of GAT-1 and GAT-3 protein content of dorsal striatum tissue taken from *Snca-/-* mice (n = 10 mice) and *SNCA+* mice (n = 7 mice). Data normalized to actin and littermate control expression. Unpaired t tests in (A-C, E,G), Paired t test in (F), Mann-Whitney tests in (H-L) and Komogorov-Smirnov tests in (J). $*P < 0.05$, $**P < 0.01$, $*** P < 0.001$, n.s. not significant.

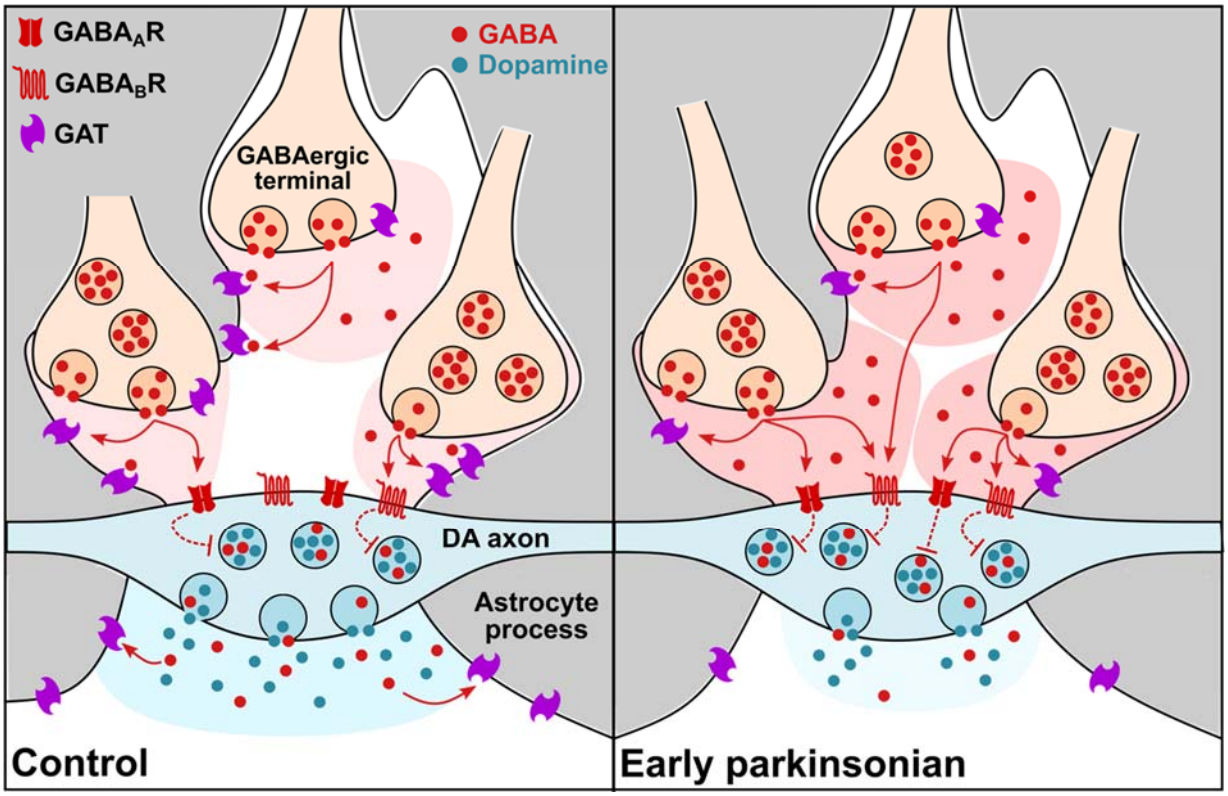

Figure 7. Augmented tonic inhibition of striatal DA release in dorsal striatum of parkinsonian mice due to reduced striatal GAT expression. Under normal circumstances (*left*), GAD-synthesized GABA is released from GABAergic striatal neurons can spillover to act at GABA receptors (GABA$_A$R and GABA$_B$R) located presumably on DA axons, inhibiting (dashed red lines) DA and GABA co-release. The level of GABA spillover and tonic inhibition of DA release is determined by the activity of GABA transporters (GATs) located on astrocytes (*gray*) and neurons, which remove GABA from the extracellular space. In a mouse model of early Parkinsonism (*right*), striatal GAT expression is downregulated in dorsal striatum, resulting in augmented tonic inhibition of DA release by GABA. Co-release of GABA from DA axons is also reduced.